Title: Nidogens are therapeutic targets for the prevention of tetanus

Authors: Kinga Bercsenyi[1,2], Nathalie Schmieg[1,2,$], J. Barney Bryson[2,$], Martin Wallace[1,2], Paola Caccin[3], Matthew Golding[1,§], Giuseppe Zanotti[3], Linda Greensmith[2], Roswitha Nischt[4] and Giampietro Schiavo[2,*]

Affiliations:

[1]Molecular Neuropathobiology Laboratory, Cancer Research UK London Research Institute, 44 Lincoln's Inn Fields, London, WC2A 3LY, UK;

[2]Sobell Department of Motor Neuroscience & Movement Disorders, UCL Institute of Neurology, University College London, WC1N 3BG London, UK;

[3]Department of Biomedical Sciences, University of Padua, Viale G. Colombo 3, 35131 Padova, Italy;

[4]Department of Dermatology, University of Cologne, Kerpener Strasse 62, 50937 Cologne, Germany

$Equal contribution

[*]Correspondence to: Prof. Giampietro Schiavo, Sobell Department of Motor Neuroscience & Movement Disorders, UCL Institute of Neurology, University College London, Queen Square, WC1N 3BG London, UK Phone: ++44 7918 738393, Fax: ++44 20 7813 3107; e-mail: giampietro.schiavo@ucl.ac.uk

Present address: [§]Centre for Microvascular Research, William Harvey Research Institute, Barts & The London School of Medicine and Dentistry, Queen Mary, University of London, London, UK

Abstract: Tetanus neurotoxin (TeNT) is amongst the most poisonous substances on Earth and a major cause of neonatal death in non-vaccinated areas. TeNT targets the neuromuscular junction (NMJ) with high affinity, yet the nature of the TeNT receptor complex remains unknown. Here, we showed that the presence of nidogens (also known as entactins) at the NMJ is the main determinant for TeNT binding. Inhibition of TeNT-nidogen interaction using small nidogen-derived peptides or genetic ablation of nidogens prevented the binding of TeNT to neurons and protected mice from TeNT-induced spastic paralysis. Our findings demonstrated the direct involvement of a protein receptor for TeNT at the NMJ, paving the way for the development of therapeutics for the prevention of tetanus by targeting this protein-protein interaction.

One Sentence Summary: Nidogens enable tetanus neurotoxin's entry into the neuromuscular junction and preventing this interaction protects mice from tetanus-induced spastic paralysis.

Main Text:

Tetanus neurotoxin (TeNT) is composed of two subunits, which perform specific functions necessary for targeting this toxin to the central nervous system (CNS) and its high potency. The heavy (H) chain mediates high-affinity binding and entry into neurons, whereas the light (L) chain causes synaptic silencing of inhibitory interneurons, which normally suppress motor neuron activity, thereby inducing spastic paralysis (1). After internalization into motor neurons, the carboxyl-terminal fragment of the H chain (H_CT) is sorted to signaling endosomes, which undergo axonal retrograde transport towards the motor neuron cell body (2). We have previously characterized the proteome of these organelles using H_CT-conjugated magnetic nanoparticles (2). This affinity approach identified a list of proteins associated with signaling endosomes, some of which were predicted to be involved in the binding and/or internalization of H_CT. We analyzed the sequences of these proteins for the presence of the tripeptide Tyr-Glu-Trp (YEW), which was previously shown to interact with the sialic acid binding site (R site) of H_CT, a region implicated in polysialogangliosides and acidic lipid binding (3, 4). In contrast, the corresponding region of botulinum neurotoxins (BoNTs) interacts with the synaptic proteins SV2A-C or synaptotagmin I/II (5-11), raising the possibility that the R site of TeNT also binds to a protein receptor.

To identify putative TeNT receptors, we selected candidates containing variants of the YEW peptide, where this motif is exposed within the lumen of signaling endosomes, a localization topologically equivalent to the extracellular domain of these proteins when localized to the plasma membrane (Table S1). A total of 35 nine-residue peptides containing the YEW motif or closely related sequences were tested for binding to H_CT using direct fluorescent binding, ELISA and peptide pull down assays (Fig. 1A; Fig. S1A,B). The interacting peptides

were then assessed for their ability to compete for H_CT binding on primary motor neurons (Fig. S1C). Peptides N1 and N2, which correspond to short sequences in nidogen-1 and nidogen-2, respectively (Table S1; Fig. S1D), were selected for further investigation as they significantly reduced H_CT binding to neurons (Fig. 1C,D; Fig. S1C). The YEW-like motif of nidogen-1 (YQW) and nidogen-2 (WSY) and their flanking residues were responsible for this interaction since single alanine mutants show reduced binding to H_CT (Fig. S1E,F) and the double alanine mutant ($N1_{AA}$; Table S1) failed to block the binding of H_CT to motor neurons (Fig. 1C,D). Furthermore, when the N1 peptide, but not $N1_{AA}$, was added to motor neurons either together with H_CT, or 10 min afterwards, it still significantly inhibited H_CT binding to these neurons (Fig. 1E,F).

We then tested whether H_CT interacts directly with full-length nidogens by incubation of immobilized HA-tagged H_CT with full-length recombinant nidogen-1 or nidogen-2, and demonstrated that both proteins directly bind to H_CT (Fig. 1B). The N1 and N2 peptide sequences of nidogen-1 and -2 played a key role in this interaction, since pre-incubating H_CT with an excess of these peptides, but not their respective mutants (Table S1), abolished this binding (Fig. 1B).

The two mammalian nidogens play partially overlapping roles in basement membrane (BM) formation and maintenance (12-14). Whilst nidogen-2 knockout (KO) mice do not display any overt phenotype, animals lacking nidogen-1 develop a progressive hind limb paralysis, indicating a role for this protein in motor neuron survival (15). Nidogens are tightly integrated within the BM, which renders them difficult to access for exogenous ligands. To determine whether the amount of cell surface-associated nidogens is the limiting factor for H_CT binding to motor neurons, we added soluble full-length nidogen-1 together with H_CT to cultured motor

neurons together with H_CT. This resulted in the binding of exogenous nidogen-1 to motor neurons (Fig. S2) and augmented the amount of cell surface-bound H_CT (Fig. 1C,D), suggesting that the addition of exogenous nidogen-1 increased the number of H_CT binding sites on the neuronal surface. This effect was dependent upon the YEW-like motif of nidogen-1, since preincubation with the N1, but not the $N1_{AA}$, peptide prevented the increased binding of H_CT (Fig. 1C,D). Co-immunoprecipitation of H_CT and endogenous nidogen-2 from motor neurons incubated with H_CT for 5 min at 37˚C (Fig. S3) suggested that the interaction between nidogens and H_CT is preserved upon entry of H_CT into endosomal compartments.

Inspection of the domain structure of nidogens revealed that the N1 and N2 peptides reside within in the globular G_2 domain (Fig. S4A; Movie S1). Molecular modeling (Fig. S4B-D) revealed that the N1 peptide, both in isolation and within the intact G_2 domain, is able to dock to the R site of H_CT, where sialic acid, disialyllactose and the YEW motif, bind (*4*). Surprisingly, the molecular surface concealed by the N1 peptide-H_CT complex constitutes more than 40% of the total peptide surface (Fig. S4C), suggesting that this interaction, which is driven by the potential formation of five hydrogen bonds and other polar interactions (Table S2), is very strong.

The G2 domain of nidogen-1 fits into a large crevice at the top of the trefoil domain of H_CT (Fig. S4B; Movie S1), concealing 1,114 $Å^2$ and 1,106 $Å^2$ of the molecular surface of H_CT and the G2 domain of nidogen-1, respectively. Complex formation is likely to be promoted by complementary electrostatic surfaces and several potential hydrogen bonds (Table S3; Fig. S4D). To confirm the validity of this structural model, we mutated several residues of the R site of H_CT that are predicted to play an important role in the formation of this complex. As shown in Fig. S5, we found that mutations of R1226, T1146 and Y1229, which form potential H-bonds with

nidogen-1 (Tables S2 and S3, respectively), as well as of other R site residues (P1212 and G1215) (16) reduce the binding of both N1 and N2 peptides. Similarly, alanine scanning of the YEW-like motif and flanking residues in the N1 and N2 peptides strongly decreased their interaction with H_CT (Fig. S1D-F), strongly supporting the validity of the model shown in Fig. S4. This mode of interaction is likely to be conserved through evolution since the human N1 and N2 peptides showed a high degree of homology to the corresponding mouse sequences and bound H_CT (Fig. S1D).

Crucially, this model predicts that the association between H_CT and nidogen-1 is unlikely to interfere with the interaction between H_CT and polysialogangliosides, which is required for TeNT binding to the neuronal surface (*3, 17*). Thus, nidogens and polysialogangliosides have the potential to bind TeNT simultaneously, and thereby fulfill the requirements for the proposed dual receptor model (18, 19), which predicts the concurrent interaction of lipid and protein receptors to TeNT and BoNTs for their high-affinity binding to neuronal membranes.

Nidogen-2 is highly enriched in the NMJ (20), and we sought to investigate whether it is localized to the specialized presynaptic BM. We injected the upper hindlimb of wild type mice with H_CT, and then immunostained cryosections of the extensor digitorum longus (EDL) muscle for choline acetyltransferase (ChAT), a motor neuron marker, and nidogen-2. This analysis revealed that H_CT binds to the presynaptic motor neuron nerve terminal, which is in close apposition to the postsynaptic acetylcholine receptor, labelled by α-bungarotoxin (α-BTx; Fig. 2A). Increased H_CT binding was detected in areas where nidogen-2 was most abundant (Fig. 2B; Movie S2), revealing a strong correlation between the nidogen-2 content and H_CT binding at the NMJ (Fig. 2C). We then assessed if these two proteins are internalized and transported together in signaling endosomes. H_CT and an antibody against nidogen-2 were added to primary motor

neurons at 37˚C and allowed to internalize. After a mild acid wash to remove all probes still bound to the neuronal surface, the internalized α-nidogen-2 was detected using fluorescently-tagged secondary antibody. The extensive co-localization between α-nidogen-2 and H_CT throughout the axonal network and cell bodies strongly indicated that these two proteins were internalized together and co-transported by the same organelles (Fig. 2D).

To further test the importance of nidogens in TeNT intoxication, we determined the susceptibility of nidogen KO mice to TeNT-induced paralysis and assessed the ability of H_CT to bind neurons and tissues derived from these mice. Compared to wild type motor neurons, nidogen-2 KO motor neurons exhibited a significantly reduced ability to bind H_CT in vitro (Fig. 3A,B). This was further verified in vivo by demonstrating that NMJ uptake of H_CT was severely impaired in levator auris longus (LAL) muscles isolated from both nidogen-1 and nidogen-2 KO mice (Fig. 3C,D). In stark contrast, the capacity of the corresponding binding fragment of BoNT/A (H_CA) to bind to nidogen null NMJ was largely unaffected (Fig. S6A). Crucially, the addition of full-length recombinant nidogen-1 restored the ability of H_CT to bind NMJs lacking nidogen-1 (Fig. S6B). This rescue was determined by the recruitment of recombinant nidogen-1 to mutant NMJs (Fig. S6B), suggesting a replenishment of H_CT acceptor sites at the synaptic cleft.

Nidogen-1 and -2 double knockout (DKO) mice show early embryonic lethality (21), precluding the derivation of motor neuron cultures from this genetic model. To overcome this limitation, we assayed H_CT uptake into isolated hindbrains of DKO embryos taken at E11.5. In contrast to control hindbrains, which displayed robust H_CT staining, hindbrains from DKO littermates were unable to bind H_CT (Fig. 3E), further indicating that nidogen-1 and -2 are essential for H_CT binding in vivo (Fig. 3F).

Since the N1 peptide inhibited H_CT binding to NMJs in whole LAL muscle preparations (Fig. 4A), we investigated the ability of the N1 peptide to prevent uptake of TeNT in vivo, using three independent assays. Firstly, full-length TeNT was injected locally into the triceps surae muscle either alone, or in combination with the N1 or $N1_{AA}$ peptide, and the effect on spastic paralysis was assessed in vivo by footprint analysis 24 h post-injection (Fig. 4B,C). TeNT caused a permanent plantar-flexion of the affected hind-paw (Movie S3) and severe gait abnormalities, with the characteristic inability to place the affected hind-paw in the former position of the ipsilateral forepaw, as occurs in normal mice (Fig. 4B,C). Strikingly, co-administration of the N1 peptide completely abolished these TeNT-induced gait abnormalities (Movie S3), whereas the $N1_{AA}$ peptide was ineffective (Fig. 4B,C).

To corroborate this finding, we quantified the protective effect of the N1 peptide by co-injecting it with TeNT and measuring the maximal force generated by the tibialis anterior (TA) muscle using in vivo isometric muscle tension physiology. The contractile force of the TeNT-injected muscle was diminished (3.11±0.88% of non-injected control) (Fig. 4D; Fig. S7A), as was the case for muscles co-injected with TeNT and the $N1_{AA}$ peptide (2.14±1.44% of non-injected control) (Fig. 4D; Fig. S7B). However, co-administration of the N1 peptide significantly abrogated the TeNT-mediated decline in contractile force compared to the other two groups (47.46 ±10.31% of non-injected control) (Fig. 4D; Fig. S7C). Similar results were obtained using phrenic nerve-hemidiaphragm preparations (22) (Fig. S7D). Together, these results confirmed the ability of the N1 peptide to prevent symptoms of tetanus in vivo.

In order to assess the susceptibility of nidogen-2 KO mice to TeNT toxicity in vivo, we injected wild type and nidogen-2 KO mice intraperitoneally with different doses of TeNT and monitored the appearance of tetanus. Nidogen-2 KO animals showed a significant delay in the

onset and progression of tetanic symptoms at lower TeNT doses (Fig. 4E). Unfortunately, the possibility to extend these assays to mice lacking nidogen-1 was precluded by the severe epileptic and paralytic phenotype affecting these animals (15).

Interestingly, some of the symptoms displayed by nidogen-2 KO mice injected with TeNT, such as keratoconjuctivitis sicca (23), resembled those of botulism, suggesting that in the absence of one of its physiological receptors, a proportion of TeNT may exploit alternative routes of entry at the NMJ, which are shared with BoNTs. Cross-talk between the two modes of entry and intracellular transport pathways taken by TeNT and BoNTs has been previously suggested (24), and is further supported by the botulism-like symptoms shown by mice injected with high doses of TeNT (25).

Since BoNTs use several SV2 isoforms as receptors (*9-11, 22*) and SV2A has been proposed as a TeNT receptor in inhibitory neurons (26), we quantified the co-localization of H_CT with SV2 isoforms in motor neurons and tested whether pre-incubation of H_CT with recombinant nidogen-1 modifies the association of H_CT with these synaptic vesicle proteins. In the absence of exogenous nidogen, SV2A showed robust co-localization with H_CT internalized for 45 min at 37°C (45%; Fig. S8A,B), whereas the co-distribution of H_CT with SV2C under these conditions was relatively minor (Fig. S8C,D). Therefore, at least a sub-pool of TeNT could be internalized via synaptic vesicle recycling at the relatively high concentrations of H_CT (40 nM) used in this assay. However, the addition of recombinant nidogen-1 caused a significant reduction in the co-localization of H_CT with SV2A (Fig. S8A,B), but not with SV2C (Fig. S8C,D). The decreased association of H_CT with SV2A in the presence of exogenous nidogen-1 is likely to be due to the increased pool of H_CT, which had accumulated in the soma during the 45 min uptake (Fig. S8A,B). Taken together, these data suggest that in the presence of nidogen-1, H_CT is

preferentially targeted to an endocytic pathway linked to axonal retrograde transport to the cell body and is not taken up by synaptic vesicle recycling.

In conclusion, we have identified the protein receptor responsible for TeNT binding and internalization at the NMJ as well as a potential mechanism to explain the overlap between the entry routes of TeNT and BoNTs (Fig. S9). Interestingly, engineered growth factors with higher affinity for the extracellular matrix (ECM) display enhanced biological activity (27), indicating that differential binding of such ligands to ECM components is crucial for their signaling and biological function (28). TeNT might exploit a similar strategy based on a very efficient capture mechanism at specialized NMJ sites rich in nidogens, which may function to concentrate TeNT as well as physiological ligands, such as neurotrophic factors, to facilitate their uptake and sorting to axonal transport organelles. At these sites, TeNT in complex with nidogens may interact with surface receptors known to bind nidogens, such as the protein phosphatase LAR (29, 30). This specialized capture mechanism is likely to be indispensable to the host cell, and this enables TeNT to be lethal at extremely low concentrations. Our study suggests that nidogens are prime therapeutic targets for suppressing the uptake of TeNT at the NMJ and its translocation to the CNS, thereby preventing its lethal effects.

Conflict of interest

The authors declare that they have no conflict of interest.

References and Notes:

1. C. Montecucco, Clostridial Neurotoxins: The Molecular Pathogenesis of Tetanus and Botulism *Curr Top Microbiol Immunol* **195**, 278 (1995).
2. K. Deinhardt *et al.*, Rab5 and Rab7 control endocytic sorting along the axonal retrograde transport pathway. *Neuron* **52**, 293-305 (2006); published online EpubOct 19 (S0896-6273(06)00640-4 [pii] 10.1016/j.neuron.2006.08.018).

3. C. Chen, Z. J. Fu, J. J. P. Kim, J. T. Barbieri, M. R. Baldwin, Gangliosides as High Affinity Receptors for Tetanus Neurotoxin. *J Biol Chem* **284**, 26569-26577 (2009); published online EpubSep 25 (Doi 10.1074/Jbc.M109.027391).
4. S. Jayaraman, S. Eswaramoorthy, D. Kumaran, S. Swaminathan, Common binding site for disialyllactose and tri-peptide in C-fragment of tetanus neurotoxin. *Proteins* **61**, 288-295 (2005); published online EpubNov 1 (10.1002/prot.20595).
5. Q. Chai *et al.*, Structural basis of cell surface receptor recognition by botulinum neurotoxin B. *Nature* **444**, 1096-1100 (2006); published online EpubDec 21 (10.1038/nature05411).
6. R. Jin, A. Rummel, T. Binz, A. T. Brunger, Botulinum neurotoxin B recognizes its protein receptor with high affinity and specificity. *Nature* **444**, 1092-1095 (2006); published online EpubDec 21 (10.1038/nature05387).
7. R. P. A. Berntsson, L. S. Peng, L. M. Svensson, M. Dong, P. Stenmark, Crystal Structures of Botulinum Neurotoxin DC in Complex with Its Protein Receptors Synaptotagmin I and II. *Structure* **21**, 1602-1611 (2013); published online EpubSep 3 (Doi 10.1016/J.Str.2013.06.026).
8. R. P. A. Berntsson, L. S. Peng, M. Dong, P. Stenmark, Structure of dual receptor binding to botulinum neurotoxin B. *Nat Commun* **4**, 2058 (2013); published online EpubJun (Artn 2058 Doi 10.1038/Ncomms3058).
9. M. Dong *et al.*, SV2 is the protein receptor for botulinum neurotoxin A. *Science* **312**, 592-596 (2006); published online EpubApr 28 (10.1126/science.1123654).
10. L. Peng, W. H. Tepp, E. A. Johnson, M. Dong, Botulinum neurotoxin D uses synaptic vesicle protein SV2 and gangliosides as receptors. *PLoS Pathog* **7**, e1002008 (2011); published online EpubMar (10.1371/journal.ppat.1002008).
11. R. M. Benoit *et al.*, Structural basis for recognition of synaptic vesicle protein 2C by botulinum neurotoxin A. *Nature* **505**, 108-111 (2014); published online EpubJan 2 (10.1038/nature12732).
12. K. Mann *et al.*, Amino acid sequence of mouse nidogen, a multidomain basement membrane protein with binding activity for laminin, collagen IV and cells. *EMBO J* **8**, 65-72 (1989).
13. M. S. Ho, K. Bose, S. Mokkapati, R. Nischt, N. Smyth, Nidogens-Extracellular matrix linker molecules. *Microsc Res Tech* **71**, 387-395 (2008); published online EpubMay (10.1002/jemt.20567).
14. J. Kruegel, N. Miosge, Basement membrane components are key players in specialized extracellular matrices. *Cell Mol Life Sci* **67**, 2879-2895 (2010); published online EpubSep (10.1007/s00018-010-0367-x).
15. L. Dong *et al.*, Neurologic defects and selective disruption of basement membranes in mice lacking entactin-1/nidogen-1. *Lab Invest* **82**, 1617-1630 (2002).
16. A. Rummel, S. Bade, J. Alves, H. Bigalke, T. Binz, Two carbohydrate binding sites in the H(CC)-domain of tetanus neurotoxin are required for toxicity. *J Mol Biol* **326**, 835-847 (2003).
17. T. Binz, A. Rummel, Cell entry strategy of clostridial neurotoxins. *J Neurochem* **109**, 1584-1595 (2009); published online EpubJun (10.1111/j.1471-4159.2009.06093.x).
18. C. Montecucco, How do tetanus and botulinum neurotoxins bind to neuronal membranes? *Trends Biochem Sci* **11**, 315-317 (1986).

19. A. Rummel *et al.*, Identification of the protein receptor binding site of botulinum neurotoxins B and G proves the double-receptor concept. *Proc Natl Acad Sci U S A* **104**, 359-364 (2007); published online EpubJan 2 (10.1073/pnas.0609713104).
20. M. A. Fox, M. S. Ho, N. Smyth, J. R. Sanes, A synaptic nidogen: developmental regulation and role of nidogen-2 at the neuromuscular junction. *Neural Dev* **3**, 24 (2008)10.1186/1749-8104-3-24).
21. B. L. Bader *et al.*, Compound genetic ablation of nidogen 1 and 2 causes basement membrane defects and perinatal lethality in mice. *Mol Cell Biol* **25**, 6846-6856 (2005); published online EpubAug (10.1128/MCB.25.15.6846-6856.2005).
22. S. Mahrhold, A. Rummel, H. Bigalke, B. Davletov, T. Binz, The synaptic vesicle protein 2C mediates the uptake of botulinum neurotoxin A into phrenic nerves. *FEBS Lett* **580**, 2011-2014 (2006); published online EpubApr 3 (10.1016/j.febslet.2006.02.074).
23. O. Suwan-apichon *et al.*, Botulinum toxin B-induced mouse model of keratoconjunctivitis sicca. *Invest Ophthalmol Vis Sci* **47**, 133-139 (2006); published online EpubJan (10.1167/iovs.05-0380).
24. L. Restani *et al.*, Botulinum neurotoxins A and E undergo retrograde axonal transport in primary motor neurons. *PLoS Pathog* **8**, e1003087 (2012); published online EpubDec (10.1371/journal.ppat.1003087).
25. M. Matsuda, N. Sugimoto, K. Ozutsumi, T. Hirai, Acute botulinum-like intoxication by tetanus neurotoxin in mice. *Biochem Biophys Res Commun* **104**, 799-805 (1982).
26. F. L. Yeh *et al.*, SV2 mediates entry of tetanus neurotoxin into central neurons. *PLoS Pathog* **6**, e1001207 (2010)10.1371/journal.ppat.1001207).
27. M. M. Martino *et al.*, Growth factors engineered for super-affinity to the extracellular matrix enhance tissue healing. *Science* **343**, 885-888 (2014); published online EpubFeb 21 (10.1126/science.1247663).
28. L. Macri, D. Silverstein, R. A. Clark, Growth factor binding to the pericellular matrix and its importance in tissue engineering. *Adv Drug Deliv Rev* **59**, 1366-1381 (2007); published online EpubNov 10 (10.1016/j.addr.2007.08.015).
29. E. Stryker, K. G. Johnson, LAR, liprin alpha and the regulation of active zone morphogenesis. *J Cell Sci* **120**, 3723-3728 (2007); published online EpubNov 1 (10.1242/jcs.03491).
30. P. O'Grady, T. C. Thai, H. Saito, The laminin-nidogen complex is a ligand for a specific splice isoform of the transmembrane protein tyrosine phosphatase LAR. *J Cell Biol* **141**, 1675-1684 (1998).
31. J. Herreros, T. Ng, G. Schiavo, Lipid rafts act as specialized domains for tetanus toxin binding and internalization into neurons. *Mol Biol Cell* **12**, 2947-2960 (2001); published online EpubOct
32. P. Emsley, K. Cowtan, Coot: model-building tools for molecular graphics. *Acta Crystallogr D Biol Crystallogr* **60**, 2126-2132 (2004); published online EpubDec (Doi 10.1107/S0907444904019158).
33. A. T. Brunger, Version 1.2 of the Crystallography and NMR system. *Nat Protoc* **2**, 2728-2733 (2007)10.1038/nprot.2007.406).
34. K. Arnold, L. Bordoli, J. Kopp, T. Schwede, The SWISS-MODEL workspace: a web-based environment for protein structure homology modelling. *Bioinformatics* **22**, 195-201 (2006); published online EpubJan 15 (Doi 10.1093/Bioinformatics/Bti770).

35. M. Kvansakul, M. Hopf, A. Ries, R. Timpl, E. Hohenester, Structural basis for the high-affinity interaction of nidogen-1 with immunoglobulin-like domain 3 of perlecan. *EMBO J* **20**, 5342-5346 (2001); published online EpubOct 1 (10.1093/emboj/20.19.5342).
36. R. J. Carter *et al.*, Characterization of progressive motor deficits in mice transgenic for the human Huntington's disease mutation. *J Neurosci* **19**, 3248-3257 (1999); published online EpubApr 15
37. J. B. Bryson *et al.*, Amyloid precursor protein (APP) contributes to pathology in the SOD1(G93A) mouse model of amyotrophic lateral sclerosis. *Hum Mol Genet* **21**, 3871-3882 (2012); published online EpubSep 1 (10.1093/hmg/dds215).
38. M. Hopf, W. Gohring, A. Ries, R. Timpl, E. Hohenester, Crystal structure and mutational analysis of a perlecan-binding fragment of nidogen-1. *Nat Struct Biol* **8**, 634-640 (2001); published online EpubJul (10.1038/89683).

Acknowledgments: We thank S. Kjaer (Cancer Research UK London Research Institute) for help with the Octet RED96 system, K_D determination and data analysis, Nicola O'Reilly and members of the Protein and Peptide Chemistry Laboratory (Cancer Research UK London Research Institute) for peptide synthesis, purification and analysis, Subramanyam Swaminathan (Brookhaven National Laboratory) for experiments aiming at the crystallization of the N1 peptide-H_CT complex, A. Rummel and T. Binz (Medizinische Hochschule Hannover) and N. Fairweather (Imperial College London) for providing access to published H_CT mutants, Isabell Koxholt (University of Cologne) for help with nidogen-1 and -2 KO mice and J.N. Sleigh (University College London) for help with statistical analyses. We also thank C. Montecucco (University of Padua), Sergej Novoselov (University College London) for constructive comments. This work was supported by Cancer Research UK (KB, NS, MG, MW and GS), by the Medical Research Council (MW), by the University of Padua (PC and GZ), and by the Deutsche Forschungsgemeinschaft (SFB 829) at the University of Cologne and the "Köln Fortune Programm" (RN). LG is the Graham Watts Senior Research Fellow, supported by the Brain Research Trust. The data presented in this manuscript are found in the main paper and the supplementary materials and methods.

Figure legends

Fig. 1. Nidogen peptides bind to H_CT and prevent its interaction with full-length nidogens in vitro. (A) Assay for peptides that bind fluorescent H_CT. The percentage of maximal binding was plotted for each peptide. The results were tested for significance between individual peptides and Tris-buffered saline (TBS) control (n=3; *, $p<0.05$; error bar: SD). **(B)** Pull down of HA-H_CT pre-incubated with full-length recombinant nidogen-1 (upper panel) or nidogen-2 (lower panel). 'Empty beads' corresponds to samples in which HA-H_CT was omitted, and 'DMSO' to samples treated with vehicle control. Both nidogen-1 and -2 bind directly to HA-H_CT, and pre-treatment with the N1 or N2 peptide blocks this interaction. In contrast, mutant peptides ($N1_{AA}$ and $N2_{AA}$) are ineffective (n=3 for both proteins). Note that the bands detected in the empty bead controls are due to the heavy chain of the capture antibody, which co-migrates with H_CT. **(C,E)** Vehicle control (H_CT alone), N1 and mutant $N1_{AA}$ peptides were either pre-incubated **(C)**, added together (**E**, 0 min) or added after a 10 min delay **(E,** 10 min) to primary mouse motor neurons treated with AlexaFluor555-H_CT in the absence or the presence of exogenous nidogen-1 **(C)** before fixing, immunostaining for βIII tubulin and imaging. Scale bar, 50 μm **(C)**, 10 μm **(E)**. **(D,F)** Quantification of the data shown in **C** and **E**. Twenty images **(D)** or 3 tile scans of 4x4 fields **(F)** were taken for each condition, and fluorescence intensity of AlexaFluor555-H_CT bound to neurons as defined by a βIII tubulin mask, was quantified. Results were tested for statistical significance (n=3; NS, non significant; **, $p<0.01$; ***, $p<0.005$; ****, $p<0.001$ error bar: SD).

Fig. 2. The nidogen-2 content of the neuromuscular junction correlates with H_CT binding and uptake. (A,B) The anterior part of the lower hindlimb of adult mice was injected with

AlexaFluor555-H_CT. After 30 min, animals were transcardially perfused; the muscles were dissected, post-fixed, sectioned and stained for choline acetyltransferase (ChAT) or nidogen-2 and AlexaFluor555-α-bungarotoxin (α-BTx, in grey) to label neuromuscular junctions (NMJs). H_CT (in red) binds to the presynaptic site of the NMJ, where ChAT (green) is localized (**A**). Note that intensely bright H_CT puncta are found in regions where nidogen-2 (green) accumulates (**B**, green). Scale bar, 10 μm. **(C)** H_CT and nidogen-2 fluorescence intensities were quantified in 50 NMJs. There is a significant correlation between the integrated intensity of both probes ($p<0.001$, Spearman coefficient 0.923). **(D)** Primary motor neurons were incubated with AlexaFluor555-H_CT and a rabbit anti-nidogen-2 antibody (for 45 min at 37 °C), acid-washed, fixed and stained with an anti-rabbit IgG antibody. H_CT and nidogen-2 co-localization was quantified and the correspondent Mander's coefficient is shown. Scale bar, 10 μm (n=3).

Fig. 3. Neurons lacking nidogens display reduced binding to H_CT. **(A,B)** Motor neurons derived from E13.5 wild type and nidogen-2 knockout (KO) mouse embryos were incubated with AlexaFluor555-H_CT (grey). Cells were fixed and fluorescence intensity was quantified in 10 images using a βIII tubulin mask (in green). Scale bar, 20 μm. The value of non-treated cells was subtracted and data analyzed (**B:** n=3; ****, $p<0.001$; error bar: SD). (**C)** Levator auris longus (LAL) muscles of wild type, nidogen-1 and -2 KO animals were incubated with HA-H_CT, fixed and stained for HA (grey) and α-BTx (in green) to identify NMJs. Scale bar, 20 μm. (**D)** Both nidogen-1 and -2 KO NMJs show a significant decrease in their ability to bind and internalize H_CT (n=3 animals per group, 20 images per animal; ****, $p<0.001$; error bar: SD). **(E)** Nidogen-1 and -2 double KO (DKO) and wild type E11.5 embryonic hindbrains were tested for H_CT binding and uptake. Scale bar, 1 mm. **(F)** Mean intensity of H_CT staining was measured and analyzed for significance (n=3 animals per group; *, $p<0.05$; error bar: SD).

Fig. 4. The N1 peptide blocks tetanic paralysis by inhibiting TeNT biding at the NMJ. (A) LAL muscles were incubated with HA-H_CT, which had been either pre-treated with vehicle control (H_CT alone), the N1 peptide, or the $N1_{AA}$ mutant in motor neuron culture medium. Muscles were then immunostained for HA and α-BTx to identify NMJs. The ratio of H_CT-positive to HcT-negative NMJs was quantified and analyzed for significance (n=3, 6 images per condition; NS, non significant; **, $p<0.01$; error bar: SD). **(B)** Footprint analysis of control mice, or of mice following injection into the gastrocnemius muscle of a sub-lethal dose of TeNT, or TeNT pre-incubated with the $N1_{AA}$ or N1 peptides. Black circles show the paw prints from the non-injected left hindlimb, while red circles mark the paw print of the TeNT-injected right hindlimb. In control and TeNT+N1-injected mice, the black and red circles overlap, whilst in TeNT- and TeNT+$N1_{AA}$-injected mice they are separated, indicating impairment in coordination due to local tetanus. **(C)** The distance between the paw prints on the injected side was measured and tested for statistical significance (n=2, 2 animals per group; NS, non significant; *, $p<0.05$; **, $p<0.01$; error bar: SD). (**D)** The tibialis anterior muscle was injected with TeNT pre-incubated with either DMSO (vehicle control), $N1_{AA}$ or N1 peptides. Following anesthesia, the tendon of this muscle was attached to a tension sensor and the peroneal nerve was stimulated. Maximal muscle force was measured, normalized to muscle weight and tested for statistical significance in control vs. injected muscle. The N1-treated group retained a significantly higher muscle force than the vehicle- or $N1_{AA}$-treated groups. (n=6 mice per group; **, $p<0.01$; error bar: SEM). (**E)** Age and weight matched nidogen-2 KO and wild type mice were injected intraperitoneally with TeNT and monitored for up to 96 h. The time of termination due to loss of righting reflex was plotted against the TeNT dose. Note that generalized tetanus in nidogen-2

KO animals is significantly delayed at lower doses (1.5 ng/kg) compared to wild type controls (n=2 experiments, minimum 2 mice per group; t-test; **, $p<0.01$; error bar: SD).

Supplementary Materials are linked to the online version of the paper at

www.sciencemag.org

Materials and Methods

Figs. S1-S9

References (31-38) [Note: The numbers refer to any additional references cited only within the Supplementary Materials]

Movie S1-S3

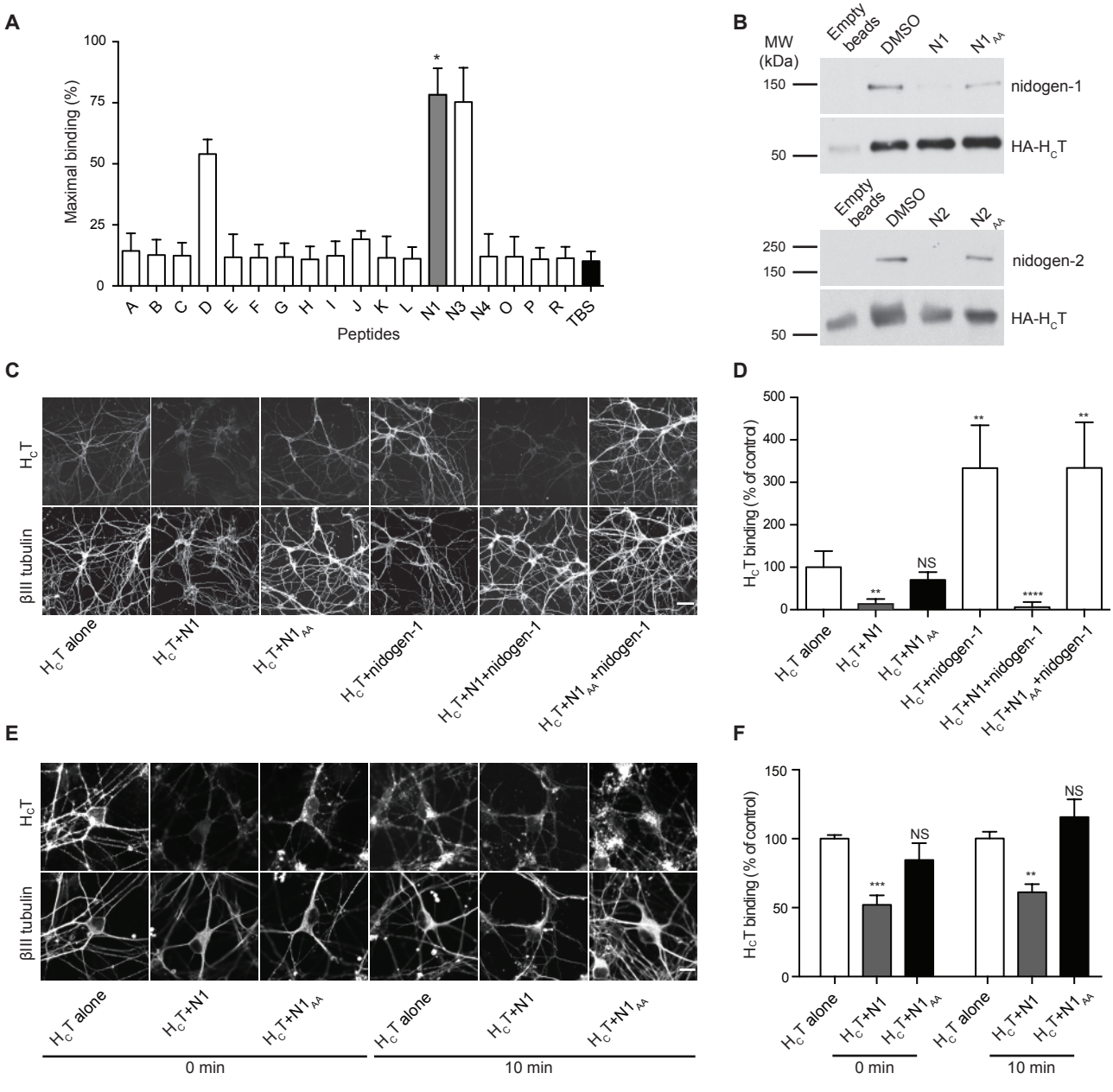

Figure 1. Bercsenyi 2014

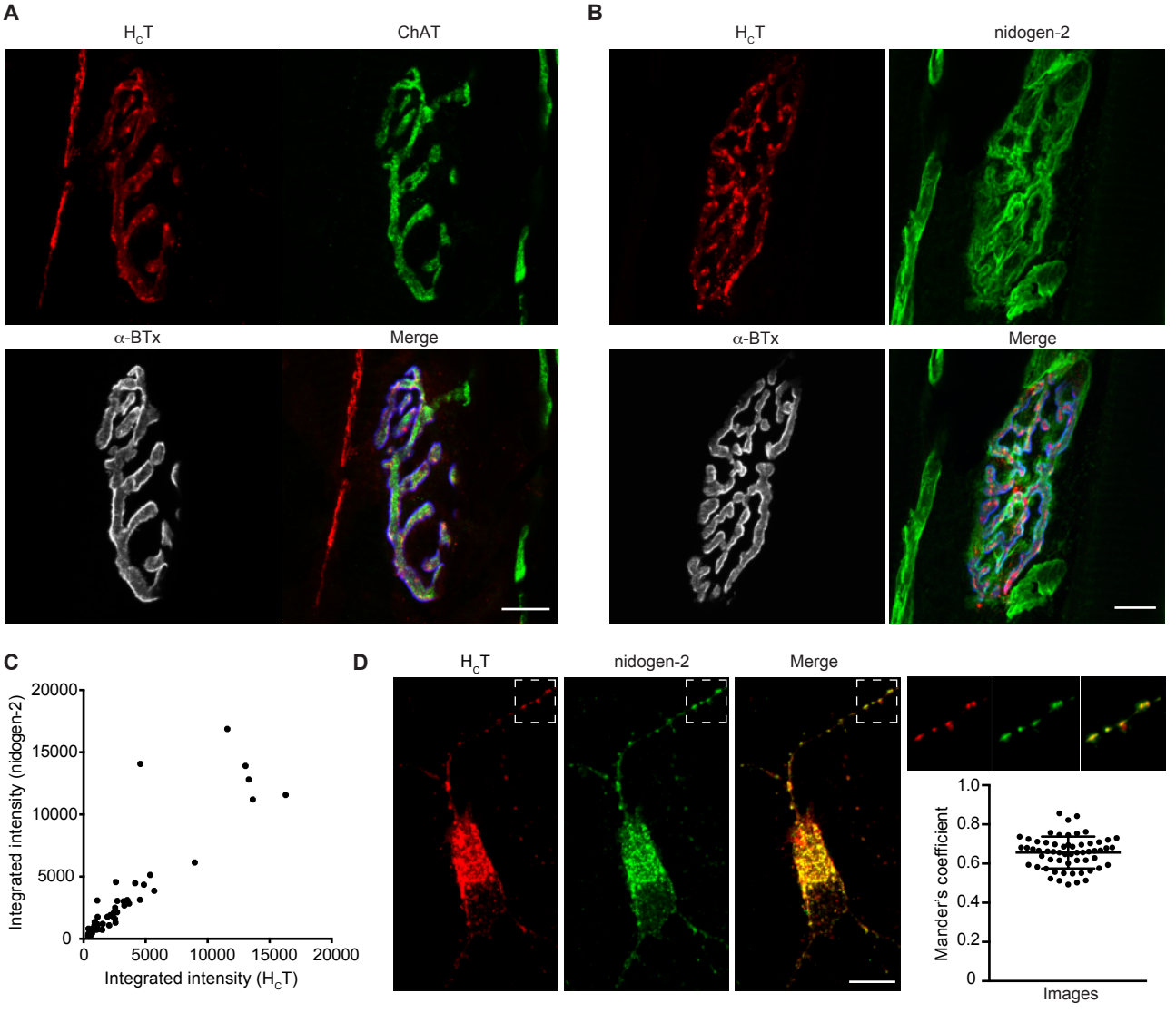

Figure 2. Bercsenyi 2014

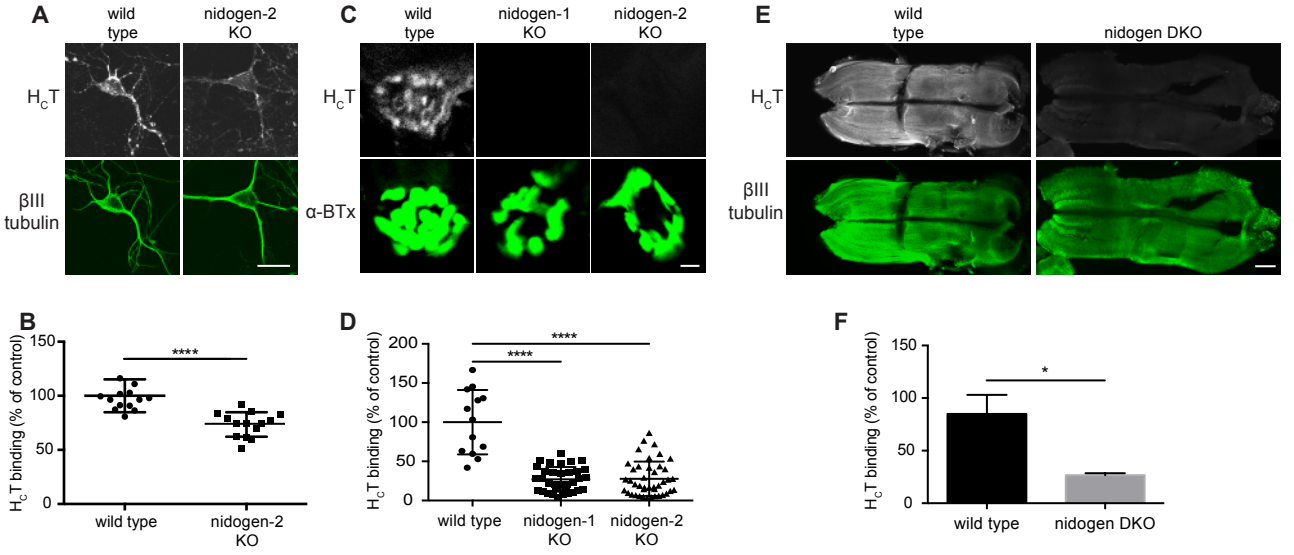

Figure 3. Bercsenyi 2014

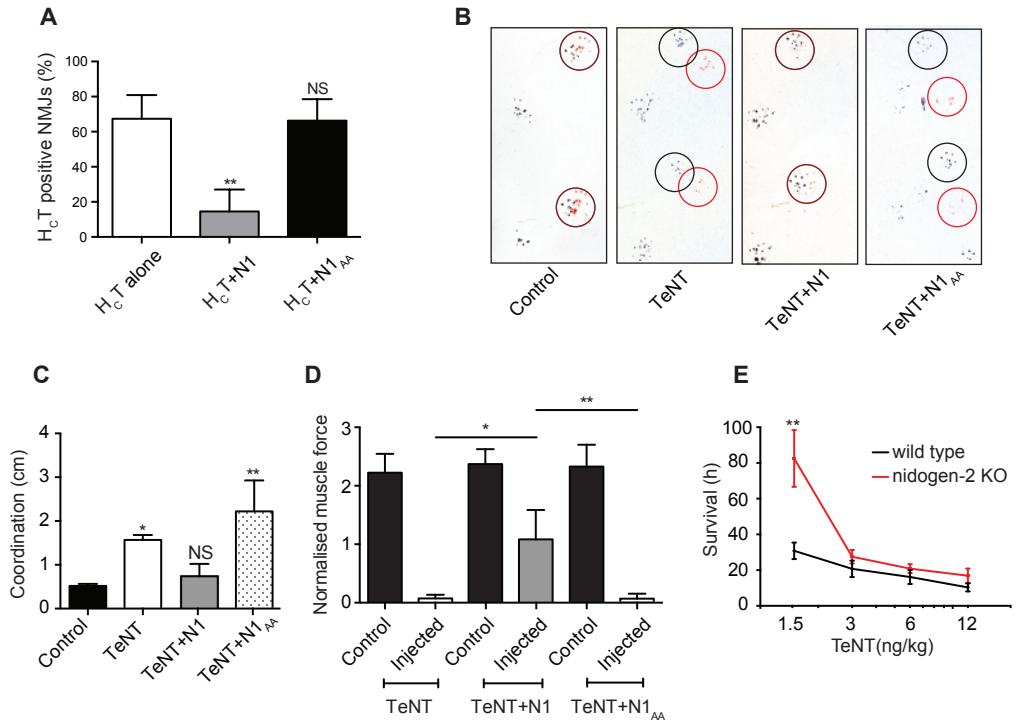

Figure 4. Bercsenyi 2014

Supplementary Materials for

Nidogens are therapeutic targets for the prevention of tetanus

Kinga Bercsenyi, Nathalie Schmieg*, J. Barney Bryson*, Martin Wallace, Paola Caccin, Matthew Golding, Giuseppe Zanotti, Linda Greensmith, Roswitha Nischt and Giampietro Schiavo

*Equal contribution

Correspondence to: Prof. Giampietro Schiavo, Sobell Department of Motor Neuroscience & Movement Disorders, UCL Institute of Neurology, University College London, Queen Square, WC1N 3BG London, UK Phone: ++44 7918 738393, Fax: ++44 20 7813 3107; e-mail: giampietro.schiavo@ucl.ac.uk

This PDF file includes:

Materials and Methods

Ethics statement

All experiments were carried out following the guidelines of the Cancer Research UK and UCL-Institute of Neurology genetic manipulation and Ethic Committees and in accordance with the European Community Council Directive of November 24, 1986 (86/609/EEC). Animal work was carried out under license from the UK Home Office in accordance with the Animals (Scientific Procedures) Act 1986 (Amended Regulations 2012).

Reagents

All reagents were obtained from Sigma, unless stated otherwise. AlexaFluor-maleimide and AlexaFluor-conjugated antibodies were purchased from Life Technologies. Recombinant nidogens were purchased from R&D Systems. H_CT (441 residues) with an improved cysteine-rich tag was prepared as previously described (24) and labeled with AlexaFluor555-maleimide following manufacturer's instructions, prior to dialysis against 10 mM HEPES-NaOH pH 7.4, 150 mM NaCl.

H_CT mutagenesis and protein expression

H_CT mutants (H_CT^{T1146A}, H_CT^{PI212W}, H_CT^{G1215F}, H_CT^{R1226F}, H_CT^{Y1229A}) were obtained by site-directed mutagenesis using PfuTurbo® DNA polymerase, according to the manufacturer's instructions using the primers listed in Table S4. Briefly, each 50 µl reaction contained 50 ng of pGEX-4T3-H_CT441 containing an improved cysteine-rich and HA tags (24), 5 µl 10× reaction buffer, 125 ng each of the forward and reverse primers, 150 µM of each dNTP, and 1 µl PfuTurbo® DNA polymerase (2.5 U/µl). PCR conditions were as follows: 95°C for 2 min, followed by 16 cycles of 95°C for 30 s, 55°C for 1 min, and 68°C for 8 min. 2 µl of each PCR reaction were transformed in E. coli XL-1 Blue and grown overnight at 37°C. DNA was purified using the QIAprep Spin Miniprep Kit (Qiagen, UK), and mutations were verified by direct sequencing.

In vitro binding assays

To screen peptides for H_CT binding, we dried 10 ng of biotin-labeled peptides and their alanine mutants on a 96-well plate overnight and incubated with Tris-buffered saline (TBS) containing 0.05% Tween and 1% bovine serum albumin (BSA) for 1 h to block unspecific interactions. Plates were then washed with TBS containing 0.05% Tween 20 (TBST) three times before adding 40 nM AlexaFluor555-H_CT in TBS and incubating it overnight at 4°C. Plates were then extensively washed with TBS and the fluorescent signal was measured using an EnVision® Multilabel Plate Reader. The highest fluorescence intensity was set at 100% for all three independent experiments. The results were plotted and tested for significance using Friedman test for the assay shown in Fig. 1A (**, $p<0.01$) followed by Dunn's multiple comparisons test against TBS (Fig. 1A). Repeated measures one-way ANOVA was used for the assay in Fig. S1E,F (****, $p<0.001$) followed by Dunnett's multiple comparisons test against N1 (E), or N2 (F).

For classic ELISA, 96-well plates were prepared as before, washed with TBST three times before adding 4 nM VSVG-H_CT (31), or 80 nM HA-H_CT (wild type and point mutants) in TBS and then incubated overnight at 4°C (VSVG-H_CT, Fig. S1A) or 1 h at

room temperature (HA-H_CT, Fig. S5B,C). Wells were extensively washed with TBS and incubated with a monoclonal mouse antibody against VSVG (P5D4, Cancer Research UK; 1:500 in TBST) or HA (12CA5; Cancer Research UK) for 2 h at room temperature. Following washes with TBST, an HRP conjugated goat anti-mouse secondary antibody (1:2,000) was added for 1 h at room temperature. Wells were then washed with TBST and blocked with TBST+1% BSA before adding ortho-phenylenediamine (OPD) until ideal color developed. The reaction was stopped with 2 M HCl and absorbance at 490 nm was measured. For the peptide screen (Fig. S1B), the results were normalized to samples where H_CT was omitted and analyzed using paired t-test. For the mutant H_CT ELISA (Fig. S5B,C) averages of triplicates within one assay were determined and the results of four independent experiments were analyzed for significance using paired t-test comparing the mutants to wild type H_CT.

For the in vitro pull down assay, the biotin-tagged peptides (20 nM) were bound to streptavidin-coated agarose beads, and used to quantify the binding between the peptides and VSVG-H_CT. We added 1 µg VSVG-H_CT to the beads, and after extensive washes in TBS, samples were analyzed by SDS-PAGE and western blotting using the P5D4 antibody. The intensity of the bands was measured in Image J and the results were analyzed by paired t- test comparing the peptide bound beads to the empty bead control.

For the in vitro immunoprecipitation, we bound HA-H_CT (1 µg) to anti-HA antibodies (2 µg) coupled magnetic Dynabeads® (10 µl; Life Technologies). After blocking with 0.1 mg/ml BSA in phosphate buffered saline (PBS) for 1 h, samples were incubated with peptides (24 µM) or DMSO for 1 h at room temperature, washed and recombinant nidogens (0.5 µg of nidogen-1 or 1 µg of nidogen-2) were added to the samples and incubated overnight at 4°C. Beads were then washed with PBS and bound proteins were analyzed by SDS-PAGE and western blotting using rabbit anti-nidogen-1 and nidogen-2 (ab14511 and ab14513 respectively, Abcam; 1:500) and rat anti-HA (3F10, Roche; 1:1,000) antibodies.

For the cell-based endogenous immunoprecipitation, HA-H_CT (80 nM) was added to primary motor neurons for 5 min at 37 °C to allow endocytosis. The cells were immediately cooled on ice, washed with ice-cold Hank's buffer and proteins were cross-linked using bis[2-(succinimidooxycarbonyloxy)ethyl]sulfone (BSOCOES; 1 mM; Thermo Scientific) in PBS for 30 min at 4°C. The reaction was stopped by the addition of 50 mM Tris-HCl pH 7.5 (final concentration). Following washes with PBS, cells were lysed on ice using IP lysis buffer (20 mM Tris-HCl pH 8, 137 mM NaCl, 1 mM EDTA, 10% glycerol, 0.5% NP40, HALT protease inhibitors (Thermo Scientific)). The lysates were cleared by centrifugation at 14000 g for 10 min and proteins binding to empty beads were cleared by incubating the samples with empty Dynabeads for 30 min at room temperature. Monoclonal mouse anti-HA antibody (12CA5; 2 µg) was cross-linked to Dynabeads (20 µl; Invitrogen) using 5 mM bis[sulfosuccinimidyl] suberate (BS3, Thermo Scientific) in 20 mM sodium phosphate, 150 mM NaCl, pH 8). After 30 min incubation at room temperature on a rotating wheel, the reaction was terminated by addition of 50 mM Tris-HCl pH 7.5 and further incubation for 15 min at room temperature. Beads were then added to lysates on a rotating wheel for 2 h at 4°C, magnetically isolated, washed and analyzed by SDS-PAGE and immunoblotting using rabbit anti-nidogen-2 and rat anti-HA (3F10, Roche; 1:1,000) antibodies.

Molecular modeling of the nidogen-1/N1 peptide-H_CT interaction

The crystal structure of H_CT with the tri-peptide YEW bound (PDB ID 1YXW) (4) was used as a template. The N1 peptide (THIYQWRQT) was constructed using Coot software (32) replacing the glutamic acid with a glutamine within the YEW peptide; the remaining residues (THI---RQT) were manually constructed and adjusted inside the crevice of H_CT. The structure was optimized by several runs of energy minimization with CNS software (33).

A model of the human nidogen-1 fragment (amino acids 389 to 661), was built by homology modeling using the Swiss-Model web server (34) based on the crystal structure of mouse nidogen-1 G2/perlecan Ig3 complex as a template (PDB code 1GL4) (35). There is 85% sequence identity between the human and mouse proteins (Fig. S1D).

The peptide 604-612 of human nidogen-1 was manually superimposed to N1 peptide in the nidogen-1-H_CT complex using Coot. The model of the two proteins was optimized by energy minimization and subjected to molecular dynamics with CNS software. Several steps of dynamics at room temperature were performed, keeping the structure of nidogen-1 fixed. The Cα atoms of H_CT were harmonically restrained during the dynamics, with the exception of residues 1142-1149 and 1212-1227 in the interaction region of the two proteins, which were left free to move.

Immunofluorescence assays on primary motor neurons

Spinal cord motor neurons were prepared from E13.5 old mouse embryos (C57/Bl6, Charles River) and plated onto poly-L-ornithine and laminin coated glass coverslips. For H_CT binding studies, wild type motor neurons were cooled on ice prior to incubation with H_CT (20 nM), which was pre-treated with either DMSO, or the N1/$N1_{AA}$ peptide (20 μM), or recombinant nidogens (1 nM), or a combination of the above for 1 h at room temperature at a molar ratio of 1:20:20,000 (recombinant nidogen-1:H_CT:N1/$N1_{AA}$ peptide). Cells were incubated with fluorescent H_CT for 10 min before washing with ice-cold Hanks' buffer (20 mM HEPES-NaOH pH 7.4, 0.44 mM KH_2PO_4 0.42 mM NaH_2PO_4, 5.36 mM KCl, 136 mM NaCl, 0.81 mM $MgSO_4$, 1.26 mM $CaCl_2$, 6.1 mM glucose) and fixing with 4% paraformaldehyde (PFA) in PBS for 15 min at room temperature. To obtain a mask for fluorescence intensity quantification, we stained the cells with a mouse monoclonal antibody against βIII tubulin (MMS-435P, Covance; 1:1,000) and an AlexaFluor488-conjugated goat anti-mouse secondary antibody (1:500). Twenty images were acquired for each condition using a Zeiss LSM510 confocal microscope equipped with a Zeiss 40x objective and analyzed for H_CT binding using Cell Profiler. The mean fluorescence intensity was plotted for each condition and statistical significance was analyzed using Kruskal-Wallis test (****, $p<0.001$) followed by Dunn's multiple comparisons test. To confirm that recombinant nidogen-1 binds to motor neurons, the cells were probed with mouse anti-His antibody (34698, Qiagen; 1:300), followed by an AlexaFluor488-conjugated goat anti-mouse secondary antibody (1:500).

To assess the ability of the N1 peptide to block H_CT accumulation when it is added to the sample after H_CT, wild type motor neurons were incubated with AlexaFluor555-H_CT, and vehicle control (DMSO) or the N1/$N1_{AA}$ peptide was added at 0 or 10 min. The cells were allowed to internalize H_CT for 45 min at 37 °C before cooling on ice, mild acid wash and fixation with 4% PFA. The cells were subjected to the same immunofluorescence protocol as above, and 4x4 tile scans were taken using a Zeiss

LSM780 confocal microscope equipped with a 63x objective. H_CT binding was analyzed using Cell Profiler. The mean intensity of H_CT alone (DMSO) was set at 100% for both the 0 and 10 min samples and the effects of the addition of $N1/N1_{AA}$ was analyzed using one-way ANOVA (***, $p<0.005$) followed by Dunnett's multiple comparisons test.

For assessing the ability of nidogen-2 KO primary motor neurons to bind H_CT, we isolated motor neurons from nidogen-2 KO and wild type E12.5 embryos and cultured them for 7-10 days (DIV 7-10). Cells were cooled on ice, and incubated with AlexaFluor555-H_CT (20 nM) for 10 min. Following a wash with ice-cold Hanks' buffer, the cells were fixed with 4% PFA in PBS for 15 min at room temperature. We stained the coverslips with mouse monoclonal antibody against βIII tubulin and an AlexaFluor488-conjugated goat anti-mouse secondary antibody (1:500). Ten images were acquired for each condition using a Zeiss LSM510 confocal microscope equipped with a Zeiss 40x objective and analyzed for H_CT binding using Cell Profiler. Following setting the level of the sample where H_CT was omitted to 0, the mean fluorescence intensity was plotted for each genotype and statistical significance was analyzed using unpaired t-test.

For co-localization studies, motor neurons were incubated with fluorescent H_CT (40 nM) together with rabbit polyclonal antibody against nidogen-2 at 37°C for 45 min, then cooled on ice and subjected to an acid wash (2 min; 100 mM citrate-NaOH, 140 mM NaCl, pH 2.0) to remove the surface bound probes before fixation with 4% PFA in PBS for 15 min at room temperature. Cells were permeabilized using 0.1% Triton X-100 in PBS for 10 min at room temperature and blocked with 5% BSA in PBS for 1 h. The primary antibody was revealed using an AlexaFluor488-conjugated goat-anti-rabbit secondary antibody.

For the SV2 co-localization studies, motor neurons were incubated either with fluorescent H_CT alone (40 nM), or together with recombinant nidogen-1 (1.6 nM; 2570-ND-050; R&D Systems) for 45 min at 37 °C. Cells were then acid washed, fixed, permeabilized and blocked as described above prior to staining with a rabbit polyclonal antibody against SV2A (SYSY119002; Synaptic System; 1:500) or SV2C (a kind gift from T. Südhof; 1:100) and a mouse monoclonal antibody against βIII tubulin. Primary antibodies were detected as described above.

Samples were imaged as before using a Zeiss 63x, Plan Apochromat oil-immersion objective. The Zeiss LSM510 (SV2) and LSM780 (nidogen-2) confocal microscopes were optimized for co-localization analysis and the pinholes were adjusted to match each other in every channel. The sampling was set to maximum and the level of co-localization was quantified using ImageJ. We determined Mander's coefficient on randomly chosen fields. For the SV2 colocalization statistical significance was assessed using unpaired t-test with Welch's correction.

Immunofluorescence assays on neuromuscular junctions and hindbrains

To determine whether nidogen-2 and H_CT colocalize presynaptically at the NMJ, we injected the tibialis anterior (TA) muscle of age and sex matched C57/Bl6 mice (n = 3) with HA-H_CT (14 µg, 4µl total volume) using a 10 µl Hamilton syringe under brief isoflurane-induced anesthesia. After 60 min animals were terminally anesthetized and transcardially perfused with saline followed by 4% PFA in 0.05 M (pH 7.8) TBS. Both the TA and extensor digitorum longus (EDL) muscles were dissected, post-fixed for 1hr in 4% paraformaldehyde in TBS and cryoprotected in 20% sucrose in TBS overnight at 4

°C. Muscles were mounted in O.C.T. (Tissue-Tek) and frozen on dry-ice before being sectioned on a cryostat (20 μm thickness) and collected onto poly-lysine coated slides. Sections were air-dried for 1 h prior to staining according to standard immunofluorescence staining protocols. Briefly, sections were washed three times with TBS, blocked with 5% normal goat serum (NGS) in TBS + 0.1% Triton X-100 before application of primary antibodies: rat anti-HA antibody (3F10, Roche; 1:100) rabbit anti-nidogen-2, goat anti-choline acetyltransferase (ChAT) (AB144P, Millipore; 1:100; blocked and diluted in donkey serum), which were diluted in TBS + 2% NGS + 0.1% Triton X-100 and incubated overnight at room temperature in a humidified chamber. After three 5 min washes with TBS, appropriate secondary antibodies were applied: AlexaFluor647 goat anti-rat; AlexaFluor488 goat anti-rabbit; AlexaFluor488 donkey anti-goat, blocked and diluted in donkey serum. Secondary antibodies were diluted (1:500) as described above, in combination with AlexaFluor555-α-bungarotoxin (Sigma; 1:1,000), and applied to sections for 1 h at room temperature, after which sections were washed three times with TBS. Coverslips were mounted with fluorescent mounting media (Dako) and slides were then imaged using a Zeiss LSM780 confocal microscope equipped with a Zeiss 40x Plan Apochromat oil-immersion objective. The integrated intensity of H_CT and nidogen-2 was tested using Spearman correlation in Graphpad Prism.

To test whether the N1 peptide is capable of blocking the entry of H_CT at the NMJ, we isolated levator auris longus (LAL) muscles from wild type animals and the samples were incubated with H_CT (20 nM), which was pre-treated with either DMSO, or the N1/$N1_{AA}$ peptide (20 μM) for 1 h at 37°C. The muscles were washed, fixed in 10% NBF overnight at 4°C, permeabilized using 0.1% Triton X-100 in PBS for 1 h at room temperature and blocked with 5% BSA in PBS for 1 h. Rat anti-HA antibody (3F10, Roche; 1:500) was added for 1 h at room temperature. The muscles were washed with PBS before the addition of AlexaFluor555-α-BTx (Sigma; 1:1,000) and goat anti-rat AlexaFluor488-IgG (1:500). The samples were mounted with Mowiol and imaged as above. We used α-BTx staining as a mask and analyzed H_CT binding by measuring the mean fluorescence intensity of the grey channel in Cell Profiler. The results were plotted and tested for significance by Kruskal-Wallis test (**, $p<0.001$) followed by Dunn's multiple comparisons test.

We isolated LAL muscles from adult nidogen-1 and -2 KO mice to assess their ability to accumulate H_CT at the NMJ. The muscles were incubated with H_CT (20 nM) in motor neuron medium for 2 h at 37 °C, then processed and imaged as above. The results were plotted and tested for significance by Kruskal-Wallis test (****, $p<0.001$) followed by Dunn's multiple comparisons test.

To test whether nidogen KO NMJs have normal synaptic vesicle recycling, the GST-tagged binding fragment of botulinum toxin A (H_CA; 12 μg in 4 μl) was injected into the TA muscle of wild type, nidogen-1 and nidogen-2 KO mice, as described above, and muscle sections were labeled with rabbit anti-GST (ab9085, Abcam; 1:100), followed by AlexaFluor488-conjugated goat anti-rabbit.

To test whether exogenous nidogen-1 can rescue the phenotype of nidogen-1 KO NMJs and restore H_CT binding, the experiment was performed as above, but histidine-tagged recombinant nidogen-1 (1 nM) was added together with HA-H_CT. To detect recombinant nidogen-1, we used mouse anti-His_5 antibody (34698, Qiagen; 1:500) and a goat anti-mouse AlexaFluor647-IgG (1:500).

We dissected hindbrains of nidogen-1 and -2 KO (DKO) embryos at E11.5 to determine whether the complete loss of nidogens affects H_CT binding. Hindbrains were incubated with AlexaFluor555-H_CT in motor neuron medium for 2 h at 37 °C, followed by 10% NBF fixation overnight at 4°C. The samples were immunostained for βIII tubulin as described above, mounted with Mowiol and imaged using a Zeiss LSM780 confocal microscope equipped with a Zeiss 20x Plan Apochromat objective. The mean grey value of the red channel was determined within the boundaries of the hindbrain in Image J, plotted and tested for significance using unpaired t-test with Welch's correction.

Hemidiaphragm assay

Mouse phrenic nerve-hemidiaphragms were dissociated from male Swiss-Webster CD1 mice weighing about 20 g and mounted in 2-4 ml of oxygenated (95% O_2, 5% CO_2) Krebs-Ringer solution of the following composition: 137 mM NaCl, 5 mM KCl, 1.8 mM $CaCl_2$, 1.0 mM $MgCl_2$, 24 mM $NaHCO_3$, 1 mM NaH_2PO_4 and 11 mM glucose, pH 7.4, at 37°C. Two innervated hemidiaphragm preparations were isolated from each animal; muscles were stretched to the optimal length for twitch response and allowed to equilibrate for at least 20 min at 37°C before the start of the experiment. The phrenic nerve was stimulated via two ring platinum electrodes with supramaximal stimuli of 10 V amplitude and 0.1 ms pulse duration with a frequency of 0.1 Hz. Muscle contraction was monitored with an isometric transducer (Harvard Apparatus); data was recorded and analyzed via an i-WORX 118 system with Labscribe software (Harvard Apparatus). TeNT aliquots (final concentration 5 nM) were preincubated with vehicle (DMSO) or with the N1 peptide (2.5 μM), corresponding to a molar ratio of 1:500 (TeNT:peptide), for 1 h at room temperature, and then added directly to tissue bath of two nerve-muscle preparations obtained from a single animal. Muscular twitch was monitored until complete paralysis. Data are expressed as time required to decrease the twitch to 50% of the initial value (paralysis half-time).

Footprint and gait analysis

Age and body mass matched C57/Bl6 male mice were injected with TeNT (1 or 2 ng/kg) preincubated with either DMSO, the N1 or the $N1_{AA}$ peptide at a molar ratio of 1: 13,800 (TeNT:peptide) for 1 h at room temperature at two different doses in the right triceps surae muscle. Mice were monitored for period of 96 h unless they reached the humane endpoint (appearance of moderate symptoms: hunched back and paralysis of rear limbs, or disappearance of the righting reflex for 30 s) earlier. We performed a footprint assay as previously described (36). To quantify the extent of paralysis, we measured the distance between the contralateral (injected side) front and hind paw prints. This parameter provides a reliable assessment of normal foot positioning during walking in mice, whereas triceps surae paralysis results in an increased distance between footprints. Data were analyzed using one-way ANOVA followed by Dunnett's multiple comparisons test to compare the groups. Following termination, triceps surae muscles were dissected and weighed to determine whether the administered dose based on total body weight was in accordance with the dose/mg muscle.

Isometric muscle tension physiology

8-week old female C57Bl6 mice received unilateral intramuscular injection into the TA muscle of TeNT (0.125 ng/kg, 4 µl injected volume per 20 g body mass), after preincubation with vehicle (DMSO), N1 or $N1_{AA}$ peptides at a molar ratio of 1:13,800 (TeNT:peptide) for 1 h at room temperature. After 24 h, under terminal anesthesia, isometric muscle tension force was recorded from the distal TA tendon following electrical stimulation (40-100 Hz, 0.02 ms square-wave pulses, for 450 ms) of the exposed sciatic nerve to induce maximal tetanic muscle contraction, as previously described (37). Contractile force of injected muscles was compared to contralateral (non-injected) TA muscle, as an internal control, and average changes within each group were analyzed using unpaired t-test.

Analysis of TeNT toxicity in nidogen-2 KO mice

Age and body mass-matched wild type and nidogen-2 KO mice were injected intraperitoneally with different doses of TeNT (1.5, 3, 6, 12 ng/kg). Mice were monitored for up to 96 h. The experiment was terminated when mice showed moderate symptoms (hunched back and paralysis of rear limbs or disappearance of the righting reflex for 30 s). The time of survival prior to termination was plotted against the administered dose of TeNT (31). The groups were analyzed using Kolmogorov-Smirnov test for each dose.

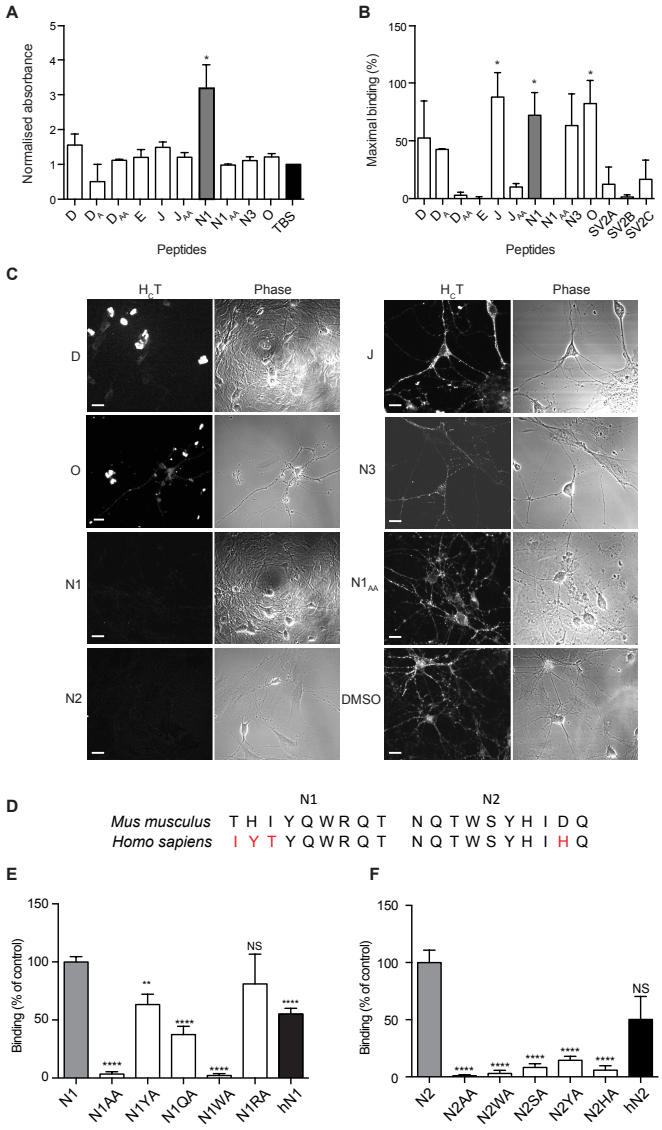

Fig. S1.

The N1 and N2 peptides block H_CT entry into primary motor neurons. (A) Peptides containing the YEW-like motif (see Table S1) were dried on 96-well plates, blocked for non–specific binding and incubated with VSVG-tagged H_CT, which was detected by ELISA using Tris-buffered saline (TBS) as a control. Statistical significance was tested between individual peptides and TBS (n=3; *, $p<0.05$; error bars: SD). **(B)** Selected biotin-tagged peptides containing variants of the YEW motif and their alanine mutants were bound to streptavidin beads and incubated with recombinant VSVG-tagged H_CT. After washing, the captured H_CT was eluted from the beads, subjected to SDS-PAGE and detected by western blotting. Band intensity was determined by densitometry using ImageJ. The results were normalized to empty bead controls and analyzed (n=3 for wild type peptides, n=2 for mutants; *, $p<0.05$; error bars: SD). **(C)** AlexaFluor555-H_CT was pre-incubated with vehicle control (DMSO), or the indicated peptides before addition to primary motor neuron cultures for 45 min at 37°C. The cells were then fixed and imaged to reveal the effect of the peptides on H_CT internalization. Scale bars, 10 μm for DMSO,

J, N2, N3; 20 μm for D, N1, $N1_{AA}$ and O. **(D)** Alignment of the sequences of mouse (Mus musculus) nidogen-1 and -2 encompassing the N1 and N2 peptides with the corresponding human (Homo sapiens) sequences. **(E,F)** Mutational analysis of the YEW-like motif and its effect on H_CT binding. Single alanine mutants of the YEW-like motif and flanking residues in the N1 and N2 peptides were immobilized on the surface of a 96-well plate and the binding of AlexaFluor555-H_CT was determined. Results were analysed for significance between the wild type (N1 and N2) peptide and the mutants (n=2; NS, not significant; **, $p<0.01$; ****, $p<0.001$, error bar: SD).

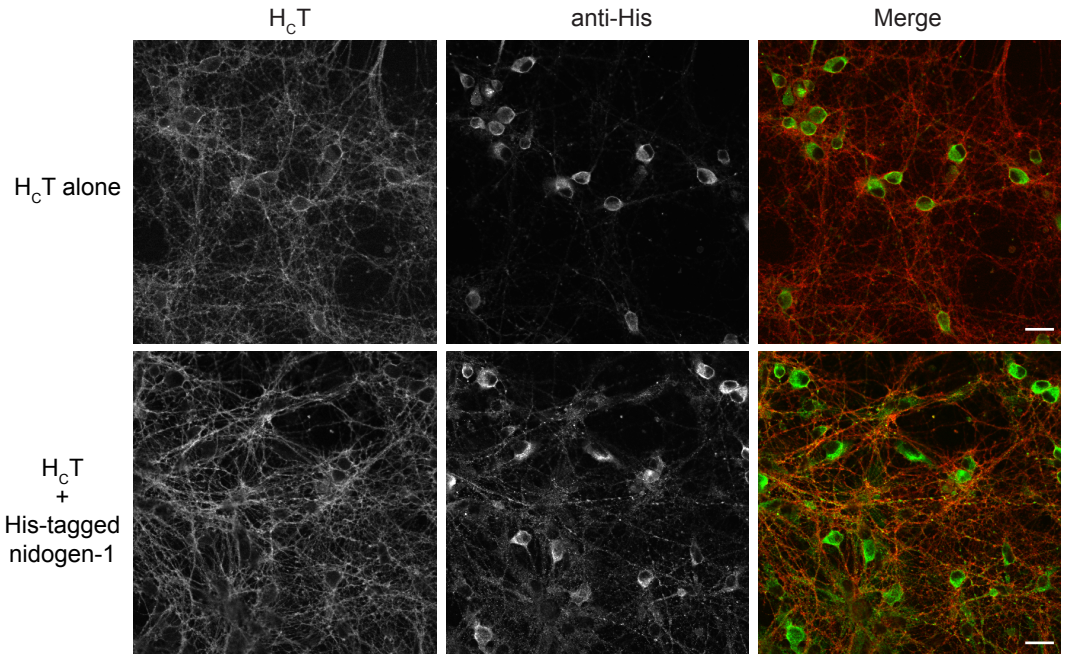

Fig. S2

Full-length recombinant nidogen-1 binds to motor neurons and recruits H_CT. AlexaFluor555-H_CT was bound to primary motor neurons for 15 min at 4°C either in the absence or presence of full-length His-tagged recombinant nidogen-1, before fixation and staining using a rabbit anti-His antibody. Note non-specific immunoreactivity of the motor neuron cell bodies. Scale bar, 20 μm.

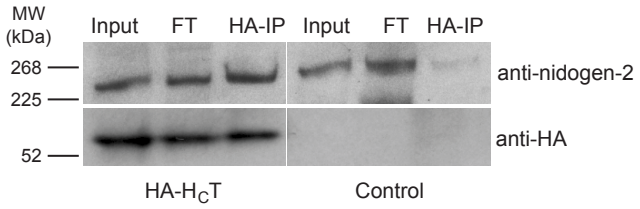

Fig. S3

Nidogen-2 interacts with HA-H$_C$T from primary motor neuron lysates. Motor neurons were incubated with HA-H$_C$T for 5 min at 37°C to allow binding and endocytosis. Since the binding of H$_C$T is detergent-sensitive, cells were pre-treated before cell lysis with a protein cross-linker (BSOCOES) to stabilize transient protein-protein interactions. Nidogen-2 was immunoprecipitated from motor neuron lysates using an anti-HA antibody and blots probed for nidogen-2 and HA-H$_C$T. In control samples, HA-H$_C$T was omitted. FT: flow through.

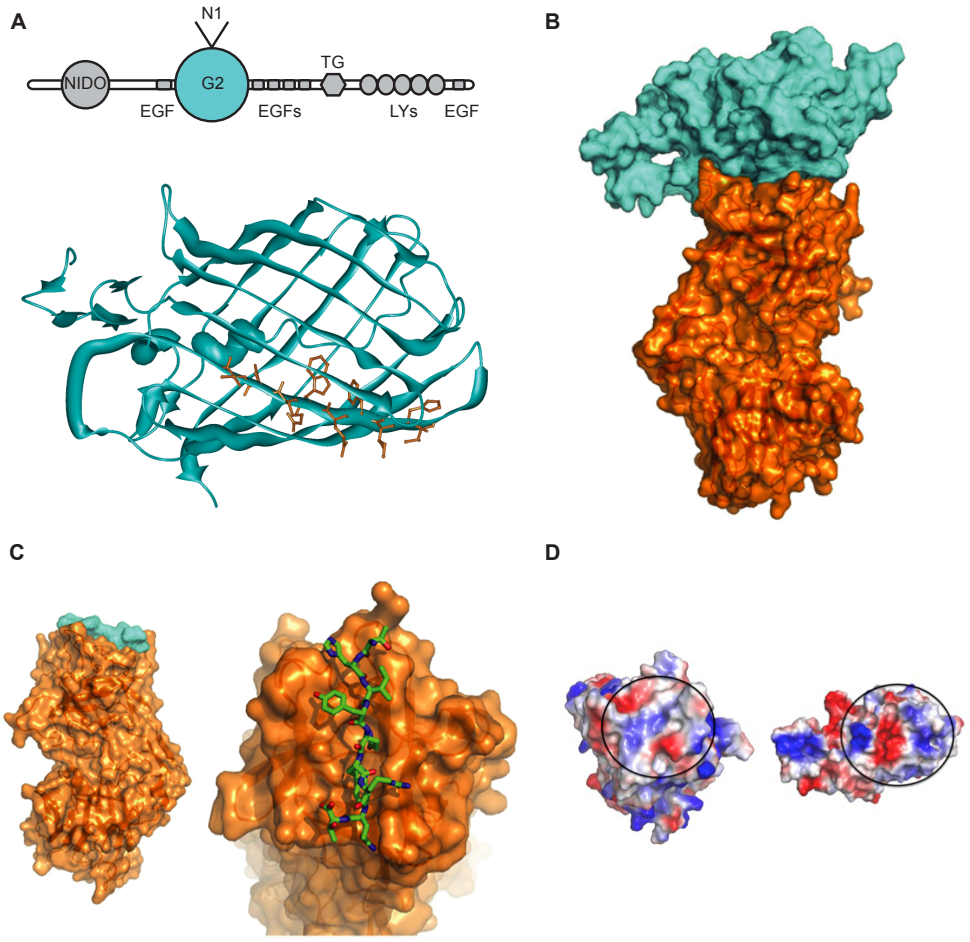

Fig. S4

Molecular modeling of the predicted interactions between the H_CT-N1 peptide and the nidogen-1 G2 domain. A) Module structure of nidogen-1 showing the position of the N1 peptide within the G2 domain of nidogen-1. Crystal structure of nidogen-1 G2 domain (cyan; bottom) with the stick model of the N1 peptide (orange; bottom, PDB ID: 1h4u (38). (B) Model of the complex of G2 domain of human nidogen-1 (cyan) and H_CT (orange). The G2 domain was manually superimposed to the N1 peptide using the graphic program Coot (32). (C) Details of the crystal structure of H_CT (orange) bound to peptide N1 (stick model; PDB code 1XYW(4)). The N1 peptide was built using Coot, the glutamic acid of the YEW sequence present in the PDB structure 1XYW was replaced with a glutamine; the remaining residues (THI---RQT) were manually built and adjusted inside the crevice of the toxin. The surface concealed by the formation of the N1 peptide-H_CT complex is 518 $Å^2$ for the H_CT domain and 592 $Å^2$ for the N1 peptide. This site is located on the opposite side of the main binding domain for polysialogangliosides, which have an established role as clostridial neurotoxin co-receptors (17), and should not interfere with polysialoganglioside binding. (D) Qualitative electrostatic potential surface of interacting regions of H_CT (left) and the nidogen-1 G2 domain (right). Circles highlight the two interacting areas, which are predicted to be complementary in terms of electrostatic charges. The bottom of the H_CT crevice is slightly positively charged, whilst the two borders are mostly negative.

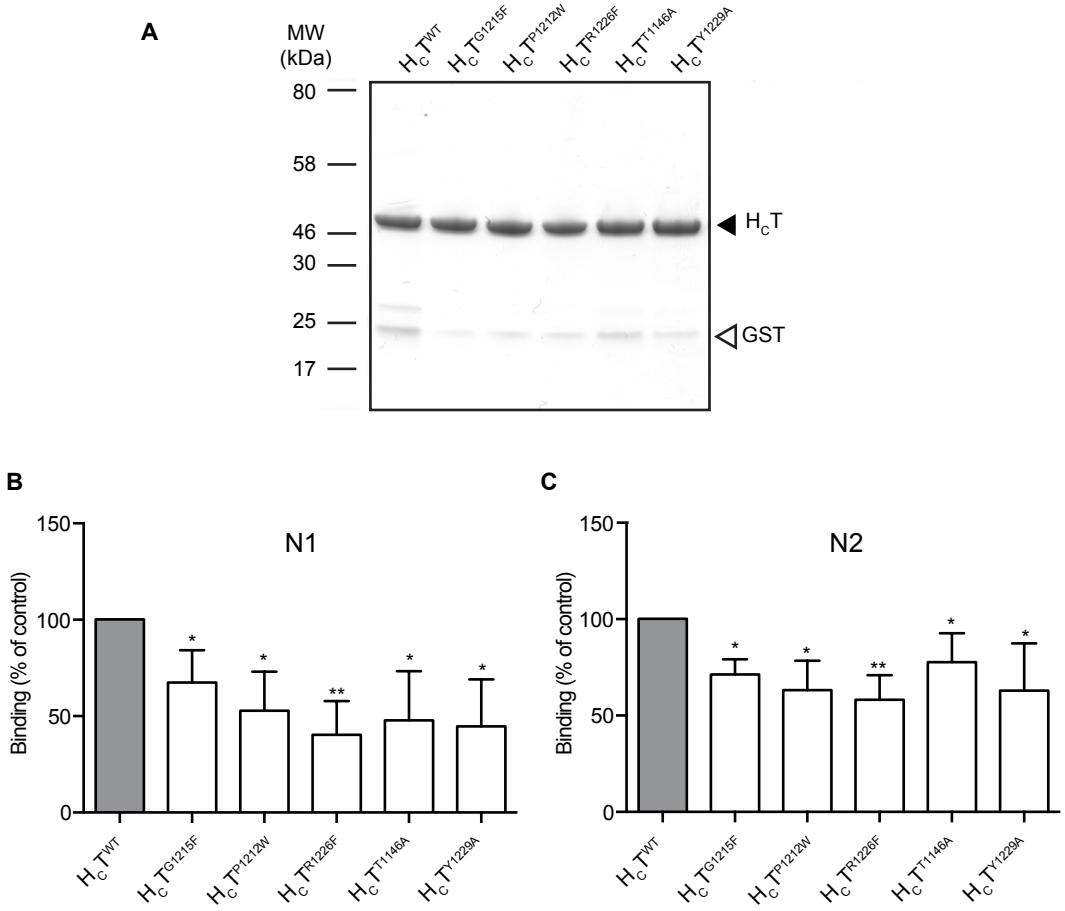

Fig. S5

The binding of H_CT to the N1 and N2 peptides is significantly reduced by point mutations in the 'R' site of H_CT. (A) Single point mutants of the R site of H_CT were generated, expressed as GST fusion proteins, and after purification and GST cleavage, subjected to SDS-PAGE to assess purity. The position of HA-H_CT (filled triangle) and a small amount of GST contaminant (empty triangle) are shown. **(B,C)** H_CT R site mutants display impaired binding to the N1 **(B)** and N2 **(C)** peptides. These peptides were immobilized on the surface of 96-well plates, blocked for non–specific binding and incubated with wild type HA-H_CT (H_CT^{WT}) and the indicated mutants. Binding was detected by ELISA using Tris-buffered saline (TBS) as a control and tested for statistical significance (n=4; *, $p<0.05$; **, $p<0.01$; error bars: SD).

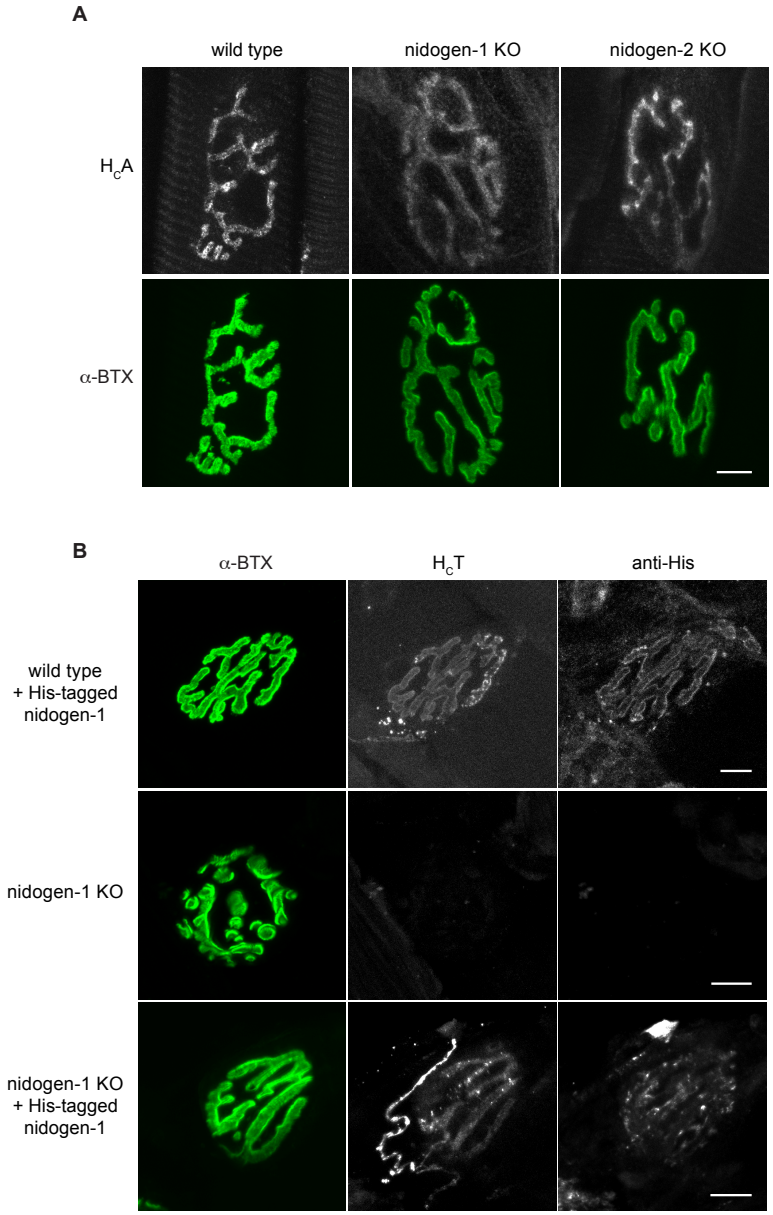

Fig. S6

Nidogen KO NMJs bind and internalise the binding fragment of botulinum neurotoxin A (H_CA), but not H_CT, unless full-length recombinant nidogen-1 is present. (A) The tibialis anterior (TA) muscle of wild type or nidogen-1 and nidogen-2 KO mice was injected with GST-H_CA. After 30 min, the animals were transcardially perfused, the muscles cryosectioned before staining for GST (grey). NMJs were labeled with AlexaFluor555-α-bungarotoxin (α-BTx; green). Scale bar, 10 µm. **(B)** Levator auris longus (LAL) muscles of wild type and nidogen-1 KO animals were incubated with HA-H_CT in the absence or the presence of full-length His-tagged recombinant nidogen-1. Muscles were fixed and stained for HA (grey, middle), His (grey, right) and α-BTx (green, left). Scale bar, 10 µm.

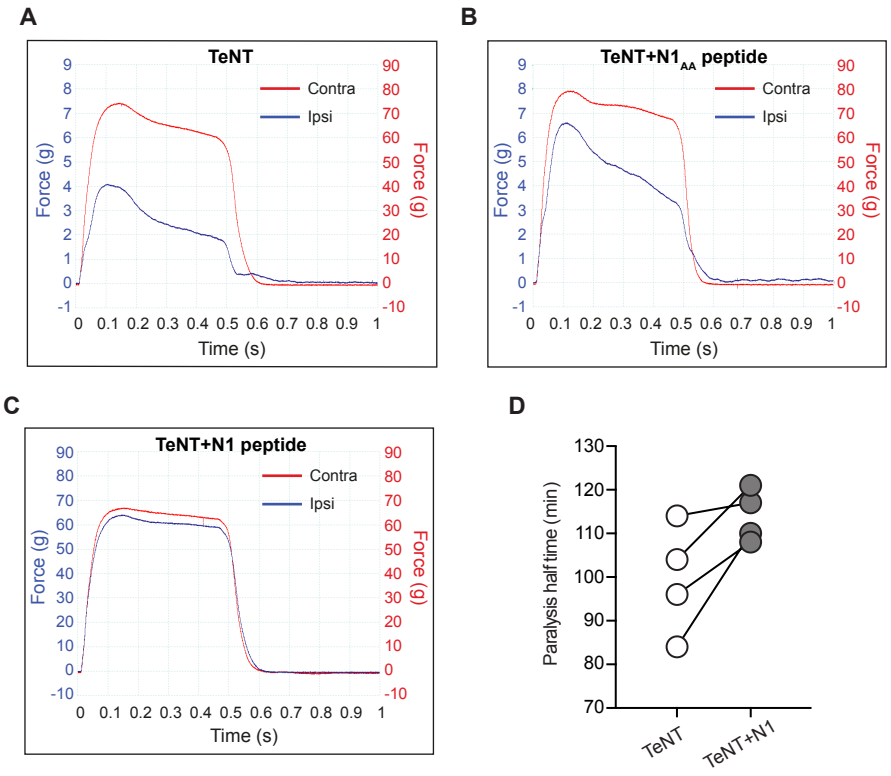

Fig. S7

The N1 peptide of nidogen-1 delays TeNT paralysis both in the TA muscle and in a phrenic nerve-hemidiaphragm preparation. (A-C) Representative isometric muscle force recordings obtained from the ipsilateral (ipsi; injected side) and contralateral (contra; non-injected internal control) TA muscles, 24 h after administration of TeNT pre-incubated with vehicle control (DMSO) **(A)**, the $N1_{AA}$ peptide **(B),** or the N1 peptide (**C**). Note that a ten fold lower scale was applied to ipsilateral and contralateral traces in **(A)** and **(B)**, while the scales are identical for both traces in **(C)** (n=6 mice per group). **(D)** TeNT pre-incubated with vehicle (DMSO) or the N1 peptide was added to the nerve-muscle preparations in Krebs-Ringer solution at 37°C. Muscle twitch was induced by nerve stimulation and paralysis times were monitored. Data is expressed as paralysis half time and reported as paired observations (n=4).

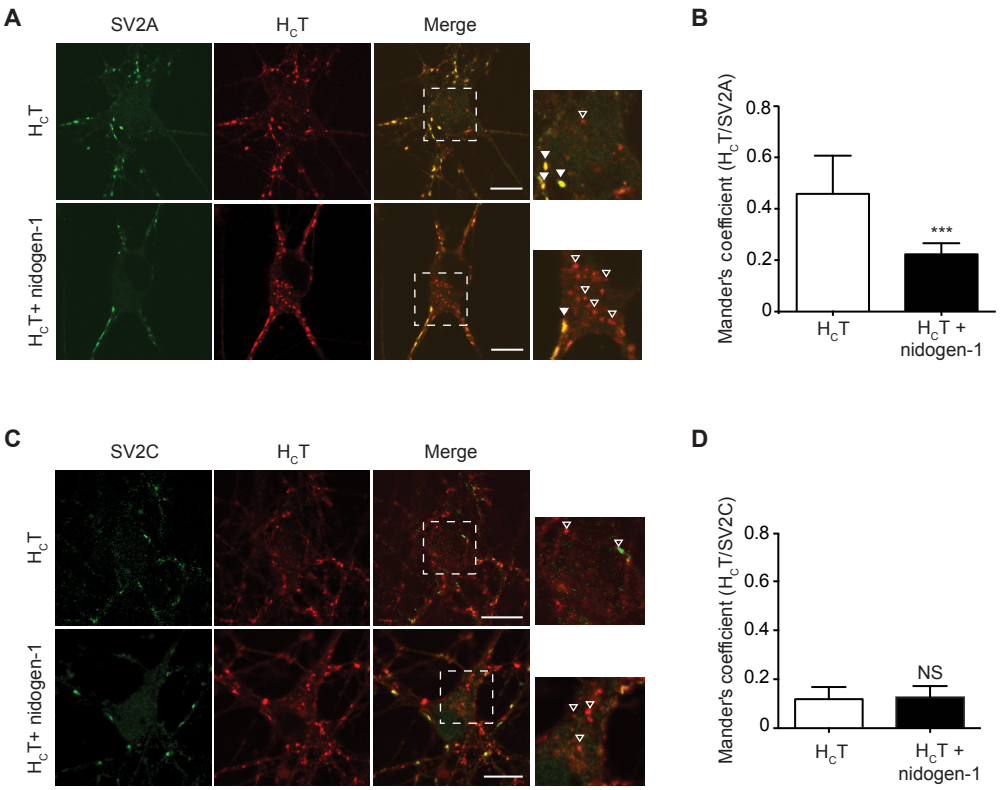

Fig. S8

Exogenous nidogen-1 decreases the colocalization between H_CT and SV2A.

(A,C) Wild type primary motor neurons were incubated either with AlexaFluor555-H_CT (shown in red; 40 nM) alone, or in the presence of full-length recombinant nidogen-1 (1.6 nM) for 45 min at 37°C. Cells were fixed and immunostained for SV2A (A) or SV2 (C) (in green). (B,D) Mander's coefficient was used as an indicator of co-localization. Significance was assessed (n=3, 10 images per condition; NS, non significant; ***, $p<0.005$; error bar: SD). Scale bar, 10 µm.

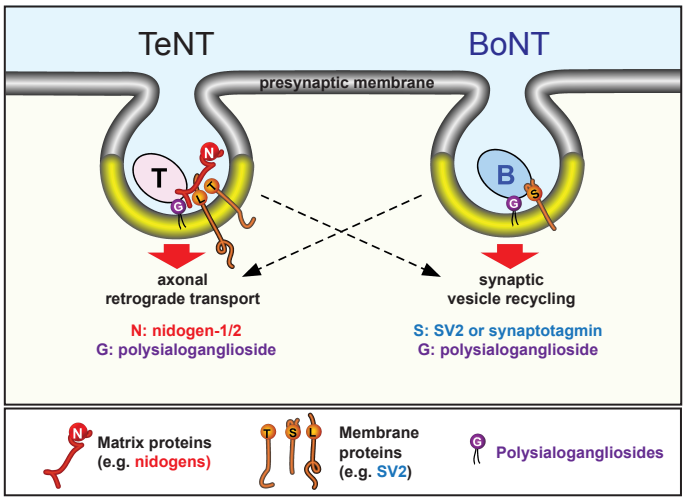

Fig. S9

Cross-talk between the uptake and trafficking routes of TeNT and BoNT. At physiological concentrations, TeNT and BoNT enter motor neurons using trafficking pathways that are mutually exclusive: TeNT is taken up by a clathrin-dependent route linked to axonal retrograde transport, whereas BoNTs are mainly internalized by the synaptic vesicle recycling pathway. Specific protein receptors localized on synaptic vesicles and exposed during synaptic activity (e.g. SV2A-C, synaptotagmin I and II) or at specialized NMJ entry sites (nidogens), participate in directing these neurotoxins to different intracellular organelles. However, high concentrations of either TeNT or BoNTs alter this equilibrium resulting in cross-talk between their respective entry routes (arrows). Addition of exogenous nidogen-1, which localize at the NMJ (Fig. S6) and are not expected to be fully sequestered by the extracellular matrix, enhance H_CT binding to motor neurons and reduce the co-localization with SV2A. This model suggests that in the presence of nidogens, H_CT is preferentially directed towards a cellular entry route linked to axonal retrograde transport and transcytosis in motor neurons, which is ultimately responsible for the targeting of TeNT to the spinal cord and the characteristic spastic paralysis of tetanus.

Table S1. **Signaling endosome-associated proteins containing variants of the YEW motif.** The sequences of the nine-residue peptides containing these motifs, which were identified in the proteome of H_CT-positive axonal signaling endosomes, are shown on the right, whilst unique identifiers for each peptide are shown on the left. The YEW-like motifs are underlined. Peptides that showed detectable binding in at least one of the assays shown in Fig. 1A and Fig. S1A,B are in bold. The N1 (nidogen-1) and N2 (nidogen-2) peptides are in red.

Peptide	Gene name	Sequence
A	Coxsackievirus and adenovirus receptor homolog	PLQFEWQKL
B	Glypican-4	DLDFEWNNF
C	Neural cell adhesion molecule 1	VAVYTWEGN
D	**Nicastrin**	**SRSFFWNVA**
D_A	Nicastrin	SRSFFANVA
D_{AA}	Nicastrin	SRSAFANVA
D3	Nicastrin	LYEYSWVQG
E	Poliovirus receptor-related protein 2/Nectin-2	PTDYDWSTT
F	Msn	KIGFPWSEI
G	Sodium/potassium-transporting ATPase subunit a1	ILEYTWLEA
H	Sodium/potassium-transporting ATPase subunit a3	ILGYTWLEA
I	Voltage-dependent calcium channel subunit a2/d1	NRTYTWTPV
J	**Vdac3 voltage gated anion channel**	**PTIYGWAVL**
J_{AA}	Vdac3 voltage gated anion channel	PTIAGAAVL
K	Voltage-dependent anion-selective channel protein 1	ETKYRWTEY
L	Voltage-dependent anion-selective channel protein 2	ETKYKWCEY
N1	**nidogen-1**	**THIYQWRQT**
$N1_{AA}$	nidogen-1	THIAQARQT
N2	**nidogen-2**	**NQTWSYHID**
$N2_{AA}$	nidogen-2	NQTASAHID
N3	**nidogen-1**	**LVGFLWKSN**
$N3_{AA}$	nidogen-1	LVGALAKSN
N_4	nidogen-1	STGYCWCVD
$ND3_{-1}$	nidogen-2	GGLFGWLFA
$ND3_{-2}$	nidogen-2	STGFCWCVD
$ND3_{-3}$	nidogen-2	KSDFCWCVD
$ND3_{-5}$	nidogen-2	KEFYHYRDS
O	**Lysosome membrane protein 2**	**GLIFTWLAC**
P	Putative phospholipase B-like 2	CPPFQWSKS
R	St13 Hsc70-interacting protein	AQPYKWRGK
SV2A	SV2A	IPHYGWSFQ
SV2B	SV2B	IPHYGWGFS
SV2C	SV2C	IPHYGWSFS

Table S2.

Supplementary Data Table 2. Potential hydrogen bond and other polar interactions between H_CT (A) and the N1 peptide from nidogen-1 (P). The predicted distance between the interacting residues is indicated. Distances must be considered as indicative, since they are based on a theoretical model. Contacts and concealed surfaces were calculated with server PISA (http://www.ebi.ac.uk). The effects of mutating the highlighted residue (R1226) on the binding to the N1 and N2 peptides are shown in Fig. S5B,C.

Bond	H_CT	Distance (Å)	nidogen-1 (N1 peptide)
H-bond			
1	A:ASP1214[OD	2.81	P:THR1[OG
2	A:ARG1226[NE	3.47	P:GLN5[OE
3	A:LYS1143[NZ]	2.91	P:GLN8[OE
4	A:LYS1143[NZ]	3.22	P:GLN8[O]
5	A:ASP1278[OD	3.08	P:GLN8[NE
Polar			
6	A:ILE1224[O]	Via a water	P:GLN5[OE
7	A:LYS1213[O]	Via a water	P:ILE3[O]
8	A:GLY1233[O]	3.15	P:HIS2[ND1

Table S3.

Potential hydrogen bonds between H_CT and the G2 domain of nidogen-1. The predicted distance between the interacting residues of H_CT (A) and the intact G2 domain of nidogen-1 (D) is indicated. Distances must be considered as indicative, since they are based on a theoretical model. Contacts and concealed surfaces were calculated as described in Table S2. The effects of mutating the highlighted residues (T1146 and Y1229) on the binding to the N1 and N2 peptides are shown in Fig. S5B,C.

Bond	H_CT	Distance (Å)	nidogen-1 (G2 domain)
1	A:ASN1144[ND2]	2.64	D:HIS 575[O]
2	A:ASN1144[ND2]	2.85	D:VAL 580[O]
3	A:THR1146[OG1]	3.48	D:THR 582[O]
4	A:ASN1216[ND2]	3.67	D:GLU 521[OE2]
5	A:TYR1229[OH]	2.91	D:SER 584[OG]
6	A:ASN1277[N]	2.63	D:THR 614[OG1]
7	A:ASN1277[ND2]	3.83	D:THR 614[O]
8	A:ILE1145[O]	3.85	D:THR 582[OG1]
9	A:LYS1213[O]	3.88	D:THR 586[OG1]
10	A:ASP1214[O]	2.82	D:ARG 610[NH1]
11	A:GLY1215[O]	2.71	D:ARG 610[NH2]
12	A:GLY1215[O]	3.56	D:THR 523[OG1]
13	A:ALA1217[O]	3.06	D:ASN 530[ND2]
14	A:TYR1229[OH]	3.74	D:THR 586[N]
15	A:TYR1229[OH]	2.94	D:GLN 608[NE2]

Table S4.
Primers used for H_CT site direct mutagenesis.

Mutant	Direction	Sequence
Y1229A	Forward	5’-CTAAGAGTAGGTGCTAATGCCCCAGGTATCCC-‘3
Y1229A	Reverse	5’-GGGATACCTGGGGATTAGCACCTACTCTTAG-3’
T1146A	Forward	5’-GTTCAATTGAAAAATATAGCAGATTATATGTATTTGAC-3’
T1146A	Reverse	5’-GTCAAATACATATAATCTGCTATATTTTTCAAATTGAAC-3’
P1212W	Forward	5’-GAGCACATTGTAGGTTATTGGAAAGATGGAAATGCC-3’
P1212W	Reverse	5’-GGCATTTCCATCTTTCCAATAACCTACAATGTGCTC-3’
G1215F	Forward	5’-GCACATTGTAGGTTATCCGAAAGATTTCAATGCCTTTAATAATC-3’
G1215F	Reverse	5’-GATTATTAAAGGCATTGAAATCTTTCGGATAACCTACAATGTGC-3’
R1226F	Forward	5’-CTTGATAGAATTCTATTCGTAGGTTATAATGCCCCAGG-3’
R1226F	Reverse	5’-CCTGGGGCATTATAACCTACGAATAGAATTCTATCAAG-3’

Movie S1

Model of the interaction of H_CT and nidogen-1. The crystal structure of H_CT (cyan) is shown bound to the N1 peptide or to human nidogen-1 (orange). The model of the molecular complex was built and minimized as described in Fig. S4.

Movie S2

Supplementary Movie 2.

Localization of nidogen-2 and H_CT at the neuromuscular junction (NMJ). 3-D rendering of a NMJ from the extensor digitorum longus muscle, fixed 1 h after H_CT injection, compiled from a z-stack of confocal images. Individual channels show fluorescent labeling of α-bungarotoxin (blue), followed by immunolabeling of nidogen-2 (green) and H_CT (red). The merged image reveals colocalization of H_CT with nidogen-2 within the NMJ. See also Fig. 2B.

Movie S3

Supplementary Movie 3.

The N1 peptide prevents TeNT-induced paralysis in vivo. Mice injected in the right triceps surae muscle with TeNT showed signs of local paralysis (the affected limb is extended) with no grip reflex. Pre-treatment of TeNT with vehicle control or the $N1_{AA}$ peptide had no effect on the progression of tetanic paralysis. In contrast, when mice were injected with TeNT pre-treated with the N1 peptide, they showed an overall normal posture, strong grip reflex and no gait abnormalities, demonstrating a blockade in TeNT-induced paralysis. See also Fig. 4B,C